nature medicine

Mfge8 promotes obesity by mediating the uptake of dietary fats and serum fatty acids

Amin Khalifeh-Soltani[1–3], William McKleroy[1–3], Stephen Sakuma[1–3], Yuk Yin Cheung[1,3], Kevin Tharp[4,5], Yifu Qiu[1], Scott M Turner[6], Ajay Chawla[1,3,7], Andreas Stahl[4,5] & Kamran Atabai[1–3]

Fatty acids are integral mediators of energy storage, membrane formation and cell signaling. The pathways that orchestrate uptake of fatty acids remain incompletely understood. Expression of the integrin ligand Mfge8 is increased in human obesity and in mice on a high-fat diet, but its role in obesity is unknown. We show here that Mfge8 promotes the absorption of dietary triglycerides and the cellular uptake of fatty acid and that Mfge8-deficient (*Mfge8*$^{-/-}$) mice are protected from diet-induced obesity, steatohepatitis and insulin resistance. Mechanistically, we found that Mfge8 coordinates fatty acid uptake through $\alpha_v\beta_3$ integrin– and $\alpha_v\beta_5$ integrin–dependent phosphorylation of Akt by phosphatidylinositide-3 kinase and mTOR complex 2, leading to translocation of Cd36 and Fatp1 from cytoplasmic vesicles to the cell surface. Collectively, our results imply a role for Mfge8 in regulating the absorption and storage of dietary fats, as well as in the development of obesity and its complications.

The metabolic syndrome, which leads to significant morbidity and mortality by increasing the risk of diabetes and cardiovascular disease, is often marked by obesity. The absorption of dietary triglycerides (TGs) with subsequent storage in adipose tissue is a key step in the development of obesity[1,2]. Under physiological conditions, cellular uptake of fatty acids occurs primarily through protein-mediated pathways consisting of a number of fatty acid transporters such as fatty acid translocase (Cd36) and fatty acid transport protein-1 (Fatp1, encoded by *Slc27a1*, here called *Fatp1*) that are expressed in tissue-specific patterns[3,4]. Translocation of these transporters from cytoplasmic vesicles to the cell membrane is the major mechanism through which the rate of fatty acid uptake can be acutely controlled in response to dietary and metabolic cues[5–7]. This process is regulated systemically by hormones and locally by muscle contraction[5,7].

Milk fat globule–EGF factor-8 (Mfge8) is a multifunctional glycoprotein originally identified as part of the milk fat globule membrane[8]. Mfge8 binds the $\alpha_v\beta_3$ (α_v and β_3 encoded by *Itgav* and *Itgb3*, respectively) and $\alpha_v\beta_5$ (β_5 encoded by *Itgb5*) integrins[9] and shares several functional similarities with Cd36. For example, like Cd36, Mfge8 regulates inflammation through integrin-mediated clearance of apoptotic cells[8,10], orchestrates clearance of spent rod photoreceptor outer segments[11,12] and binds collagen[13,14]. Mfge8 has a number of additional functions, including regulation of smooth muscle calcium sensitivity[15], neovascularization[16] and inhibition of nuclear factor-κB activation after integrin ligation[15,17].

Several recent observations suggest a role for Mfge8 in obesity and insulin resistance. The *MFGE8* gene is located in a region linked with eating behaviors and susceptibility to obesity in humans[18,19]. The expression of MFGE8 and the α_v and β_5 integrin subunits are increased in adipose tissue of obese humans[20]. In mouse models of obesity, Mfge8 expression is markedly induced in white adipose tissue after weight gain[21]. Further, circulating Mfge8 concentrations are elevated in patients with diabetes[22,23] and correlate with the extent of hemoglobin glycosylation[23].

The overlapping functions of Mfge8 and Cd36, the role of Cd36 in fatty acid uptake and the increased expression of Mfge8 in obese adipose tissue led us to examine whether Mfge8 regulated fatty acid uptake. We report here that Mfge8 increases fatty acid uptake in multiple organ systems, leading to expansion of adipose tissue, obesity and insulin resistance when mice are on a high-fat diet (HFD).

RESULTS

Mfge8 promotes fatty acid uptake

To evaluate the effect of Mfge8 on fatty acid uptake, we quantified the effect of recombinant Mfge8 (rMfge8) on uptake of a boron-dipyrromethene (BODIPY) fatty acid analog[24] by 3T3-L1 adipocytes. Treatment with rMfge8 increased fatty acid uptake in a dose-dependent fashion (**Fig. 1a**,**b**), whereas a recombinant construct with a point mutation changing the integrin-binding arginine-glycine-aspartate (RGD) sequence of Mfge8 to arginine-glycine-glutamate (RGE) had no effect (**Fig. 1a**,**b**). 3T3-L1 cells treated with rMfge8 during the process of differentiation from fibroblasts to adipocytes had greater TG content 2, 4, 6 and 8 d after treatment (**Fig. 1c**).

Primary adipocytes from *Mfge8*$^{-/-}$ mice isolated from epididymal white adipose tissue (eWAT) expressed Mfge8 and had similar viability as those of wild-type (WT) controls (**Supplementary Fig. 1**).

[1]Cardiovascular Research Institute, University of California, San Francisco, San Francisco, California, USA. [2]Lung Biology Center, University of California, San Francisco, San Francisco, California, USA. [3]Department of Medicine, University of California, San Francisco, San Francisco, California, USA. [4]Metabolic Biology, University of California, Berkeley, Berkeley, California, USA. [5]Department of Nutritional Sciences and Toxicology, University of California, Berkeley, Berkeley, California, USA. [6]KineMed Inc., Emeryville, California, USA. [7]Department of Physiology, University of California, San Francisco, San Francisco, California, USA. Correspondence should be addressed to K.A. (kamran.atabai@ucsf.edu).

Received 13 September 2013; accepted 11 December 2013; published online 19 January 2014; doi:10.1038/nm.3450

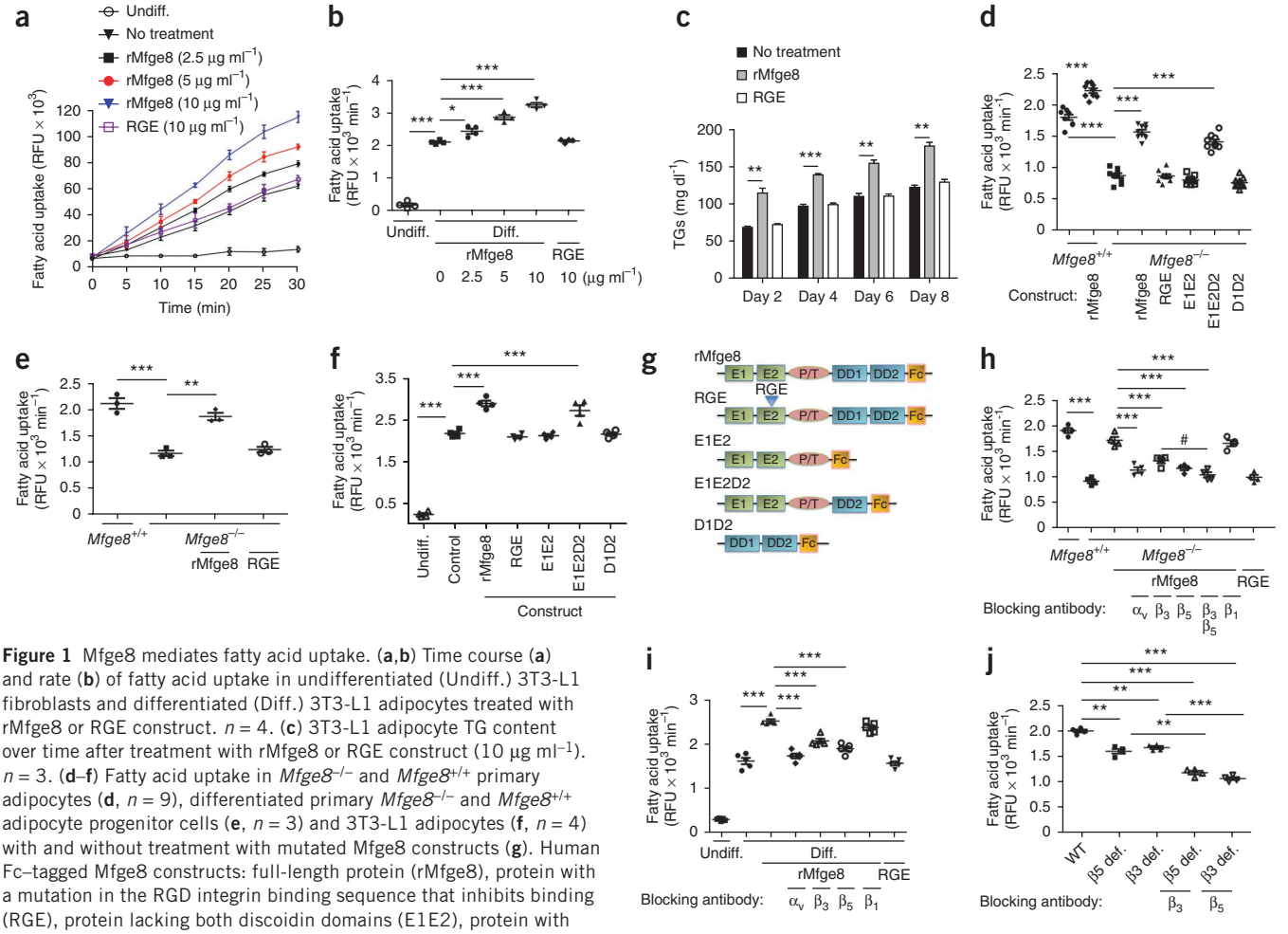

Figure 1 Mfge8 mediates fatty acid uptake. (**a**,**b**) Time course (**a**) and rate (**b**) of fatty acid uptake in undifferentiated (Undiff.) 3T3-L1 fibroblasts and differentiated (Diff.) 3T3-L1 adipocytes treated with rMfge8 or RGE construct. $n = 4$. (**c**) 3T3-L1 adipocyte TG content over time after treatment with rMfge8 or RGE construct (10 μg ml^{-1}). $n = 3$. (**d**–**f**) Fatty acid uptake in *Mfge8*$^{-/-}$ and *Mfge8*$^{+/+}$ primary adipocytes (**d**, $n = 9$), differentiated primary *Mfge8*$^{-/-}$ and *Mfge8*$^{+/+}$ adipocyte progenitor cells (**e**, $n = 3$) and 3T3-L1 adipocytes (**f**, $n = 4$) with and without treatment with mutated Mfge8 constructs (**g**). Human Fc–tagged Mfge8 constructs: full-length protein (rMfge8), protein with a mutation in the RGD integrin binding sequence that inhibits binding (RGE), protein lacking both discoidin domains (E1E2), protein with only the second discoidin domains (E1E2D2) and protein lacking both EGF-like domains (D1D2). (**h**,**i**) Effect of integrin-blocking antibodies on fatty acid uptake in *Mfge8*$^{-/-}$ adipocytes (**h**, $n = 3$ or 4) and in 3T3-L1 adipocytes (**i**, $n = 5$) treated with rMfge8. (**j**) Fatty acid uptake in β_5-deficient (β_5 def.) and β_3-deficient (β_3 def.) primary adipocytes with and without the addition of integrin-blocking antibodies. $n = 4$. Male mice were used for all experiments. $^*P < 0.01$, $^{**}P < 0.001$, $^{***}P < 0.0001$. Data are expressed as mean ± s.e.m. Each replicate represents an independent experiment. One-way analysis of variance (ANOVA) with *post hoc* Bonferroni *t*-test was used for all statistical analyses except **c**, where a Student's *t*-test was used. RFU, relative fluorescence unit.

Primary adipocytes and differentiated adipocyte progenitors from subcutaneous white adipose of *Mfge8*$^{-/-}$ mice tissue had impaired fatty acid uptake (**Fig. 1d**,**e** and **Supplementary Fig. 1f**,**g**) compared with WT controls. Treatment with rMfge8 rescued impaired fatty acid uptake in adipocytes from *Mfge8*$^{-/-}$ mice and increased fatty acid uptake in adipocytes from WT mice (**Fig. 1d**,**e**). The effect of rMfge8 on adipocyte fatty acid uptake required at least one of the discoidin domains of Mfge8 (**Fig. 1d**,**f**,**g**). Treatment of 3T3-L1 adipocytes with cyclic RGD did not induce an increase in phosphorylation of Akt (encoded by *Akt1*) or fatty acid uptake (**Supplementary Fig. 1g**).

Blocking antibodies to the α_v, β_5 or β_3 integrin subunits or both the β_3 and β_5 integrin subunits inhibited the higher rate of fatty acid uptake induced by rMfge8 treatment (**Fig. 1h**,**i** and **Supplementary Fig. 1h**). Mfge8 expression increased during 3T3-L1 differentiation, whereas expression of αv, β_3 and β_5 integrin subunits was stably persistent (**Supplementary Fig. 1i**). Adipocytes from β_5- and β_3-deficient mice had impaired fatty acid uptake (**Fig. 1j**), which was further reduced with the addition of a blocking antibody to the β_3 integrin subunit in adipocytes from β_5-deficient mice and vice versa.

Primary hepatocytes and cardiac mycocytes expressed Mfge8, and cell viability after harvest was similar between *Mfge8*$^{-/-}$ mice and WT controls (**Supplementary Fig. 1**). Hepatocytes and cardiac myocytes from *Mfge8*$^{-/-}$ mice had impaired fatty acid uptake compared with WT controls, which was rescued with rMfge8 (**Supplementary Fig. 2a**–**d**). Treatment with rMfge8 also increased fatty acid uptake in HepG2 cells, a human hepatocellular carcinoma cell line (**Supplementary Figs. 1** and **2e**–**g**).

Mfge8 mediates absorption of dietary fat

Mfge8$^{-/-}$ mice had lower small intestinal TG content as compared with WT controls (**Fig. 2a**). Primary enterocytes expressed Mfge8, and cell viability after harvest was similar between *Mfge8*$^{-/-}$ mice and WT controls (**Supplementary Fig. 1**). Primary enterocytes from *Mfge8*$^{-/-}$ mice had impaired *in vitro* fatty acid uptake (**Fig. 2b** and **Supplementary Fig. 2h**) that was rescued with the addition of rMfge8. *Mfge8*$^{-/-}$ mice had lower serum TG concentrations as compared with WT controls after olive oil gavage. Adding rMfge8, but not RGE, to olive oil raised serum TG concentrations (**Fig. 2c**). Liver TG concentrations after olive oil gavage were lower in *Mfge8*$^{-/-}$ mice as compared with WT

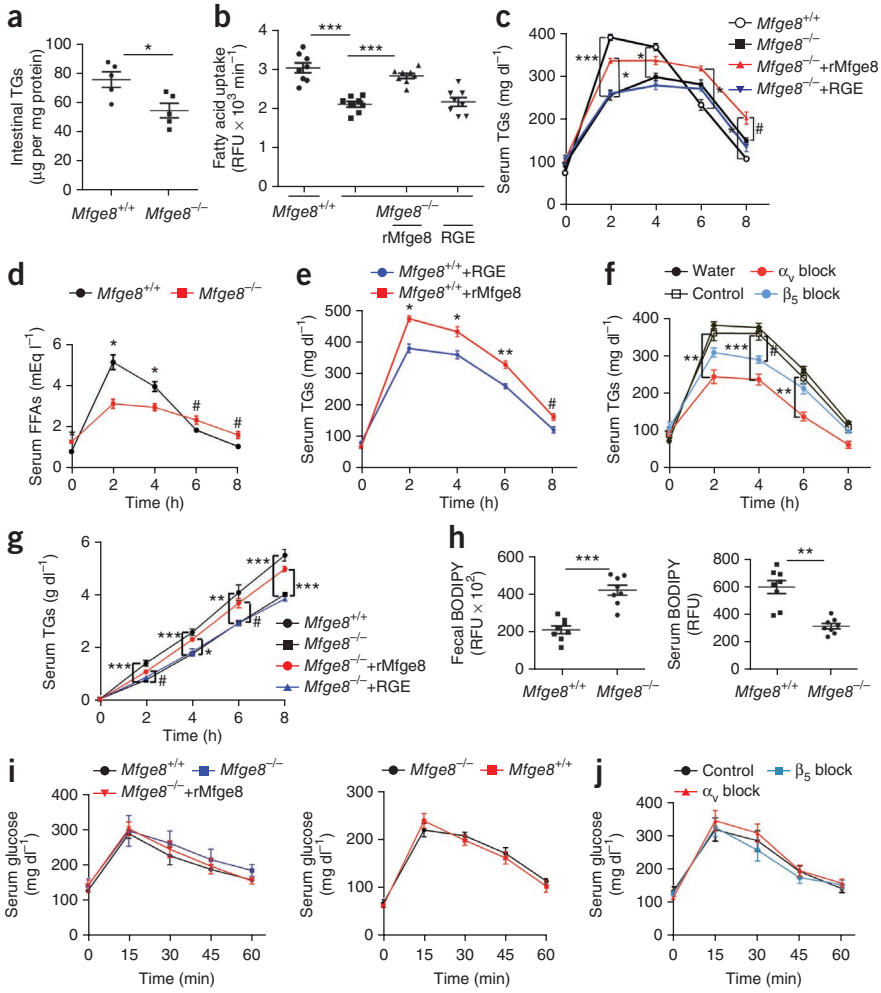

Figure 2 Mfge8 mediates absorption of dietary fats. (**a**) TG content of small intestinal tissue from *Mfge8*$^{+/+}$ and *Mfge8*$^{-/-}$ mice. $n = 5$. (**b**) Fatty acid uptake in primary *Mfge8*$^{+/+}$ and *Mfge8*$^{-/-}$ enterocytes and *Mfge8*$^{-/-}$ enterocytes treated with rMfge8. $n = 8$. Each replicate represents an independent experiment. (**c**) Serum TG after oral gavage of *Mfge8*$^{+/+}$ and *Mfge8*$^{-/-}$ mice with olive oil or olive oil mixed with rMfge8. $n = 6$ (rMfge8 treated), 7 (RGE treated) and 8 (*Mfge8*$^{+/+}$ and *Mfge8*$^{-/-}$). Results represent 2 independent experiments. (**d**) Serum FFA concentrations in *Mfge8*$^{+/+}$ *and Mfge8*$^{-/-}$ mice after olive oil gavage. $n = 5$. (**e**) Effect of rMfge8 on serum TG concentrations after olive oil gavage in *Mfge8*$^{+/+}$ mice. $n = 5$. (**f**) Effect of oral integrin-blocking antibodies before olive oil gavage on serum TG concentrations. $n = 4$ for all except β_5 block, where $n = 5$. (**g**) Serum TG concentrations after olive oil gavage and i.p. administration of Triton WR-1339. $n = 8$. (**h**) Fecal and serum BODIPY concentrations in *Mfge8*$^{+/+}$ and *Mfge8*$^{-/-}$ mice after gavage with a mixture of BODIPY fatty acid analog and a nonabsorbable rhodamine-PEG. $n = 8$. Results represent 3 independent experiments. (**i**) Serum glucose concentrations after a 4-h (left) and 18-h (right) fast in *Mfge8*$^{+/+}$ and *Mfge8*$^{-/-}$ mice gavaged with a glucose bolus and in *Mfge8*$^{-/-}$ mice gavaged with glucose mixed with rMfge8. $n = 5$. (**j**) Effect of integrin-blocking or control antibodies on glucose absorption by *Mfge8*$^{+/+}$ mice after glucose gavage. Male mice were used in **a**, **b**, **d** and **e**, and female mice were used for all remaining panels. *In vivo* experiments were performed once in **e**, **f**, **i**, and **j**, 2 independent times in **c**, **d** and **g** and 3 independent times in **h**. $^{\#}P < 0.05$, $^{*}P < 0.01$, $^{**}P < 0.001$, $^{***}P < 0.0001$. Data are expressed as mean ± s.e.m. One-way ANOVA with *post hoc* Bonferroni *t*-test was used for all statistical analyses except **a** and **h**, where a Student's *t*-test was used.

controls and increased with rMfge8 treatment (**Supplementary Fig. 3a**). Serum concentrations of Mfge8 were undetectable after treatment with oral gavage in *Mfge8*$^{-/-}$ mice (**Supplementary Fig. 3b**). Serum free fatty acid (FFA) concentrations were lower 2 and 4 h after and higher 6 and 8 h after olive oil gavage in *Mfge8*$^{-/-}$ mice as compared with WT mice (**Fig. 2d**). Treatment with rMfge8 resulted in higher TG concentrations in WT mice after olive oil gavage (**Fig. 2e**).

The administration of an α_v-blocking or a β_5-blocking antibody by gavage 30 min before receiving an olive oil bolus resulted in lower serum TG concentrations, enterocyte TG content and hepatic TG content in WT mice as compared with WT mice treated with control antibody (**Fig. 2f** and **Supplementary Fig. 3c**,**d**). Serum TG concentrations were lower after olive oil gavage and intraperitoneal (i.p.) injection of the lipoprotein lipase inhibitor Triton WR-1339 in *Mfge8*$^{-/-}$ mice as compared with WT mice (**Fig. 2g**).

Mfge8$^{-/-}$ mice had greater fecal BODIPY concentrations coupled with lower serum BODIPY concentrations as compared with WT controls after gavage of BODIPY fatty acid analog coupled with a nonabsorbale rhodamine-polyethylene glycol (PEG) (**Fig. 2h**). Fecal rhodamine-PEG concentrations were similar in *Mfge8*$^{-/-}$ mice and WT controls (**Supplementary Fig. 3e**).

Serum glucose concentrations after glucose gavage were similar in *Mfge8*$^{-/-}$ mice and WT controls after a 4- or 18-h fast (**Fig. 2i**,**j**). Serum glucose after gavage in WT mice was not affected by antibodies blocking the α_v or β_5 integrin subunits (**Fig. 2j**). Glucose uptake by 3T3-L1 adipocytes *in vitro* was also unaffected by rMfge8 (**Supplementary Fig. 3f**). The histology of the small intestine and ZO-1 expression were similar in *Mfge8*$^{-/-}$ mice as compared with WT controls (**Supplementary Fig. 3g**,**h**), indicating that intestinal barrier integrity was unaffected by Mfge8 deficiency. Serum rhodamine-PEG concentrations after oral gavage were barely detectable and were similar in *Mfge8*$^{-/-}$ mice and WT controls (**Supplementary Fig. 3i**).

Mfge8 mediates clearance of serum TGs

We next measured serum TG and FFA concentrations after i.p. injection of an olive oil bolus. Serum TG and FFA concentrations were similar 1 h after i.p. injection of olive oil but were elevated 2, 3 and 4 h after injection in *Mfge8*$^{-/-}$ mice as compared with WT controls (**Fig. 3a**). *Mfge8*$^{-/-}$ mice had similar TG and FFA concentrations in the fed state and higher serum FFA and TG concentrations after a 24-h fast as compared with WT controls (**Fig. 3b**).

After i.p. injection of BODIPY, *Mfge8*$^{-/-}$ mice had higher serum BODIPY concentrations and reduced BODIPY concentrations in the eWAT, liver and heart as compared with WT mice (**Fig. 3c**,**d** and **Supplementary Fig. 4a–d**). After i.p. injection of [^{14}C]oleic acid, *Mfge8*$^{-/-}$ mice had higher serum ^{14}C concentrations and lower tissue

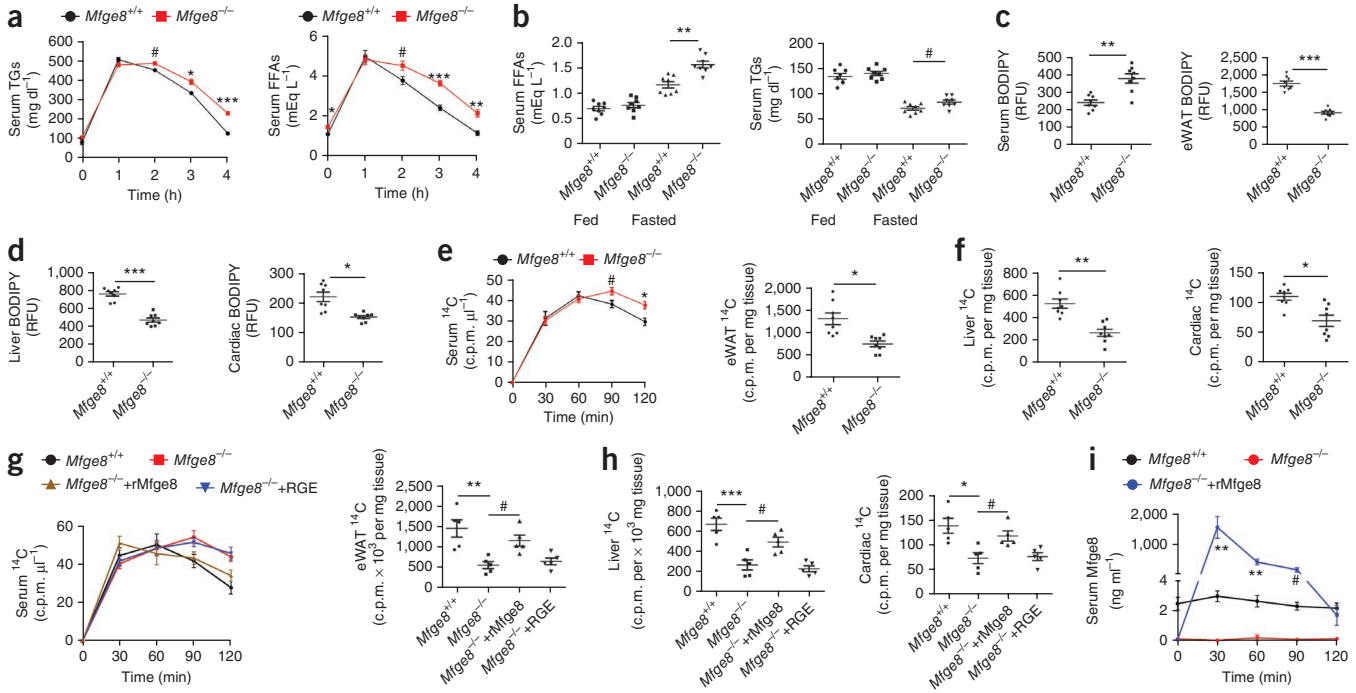

Figure 3 Mfge8 mediates fatty acid clearance from serum and deposition in peripheral organs. (**a**) Serum TG and FFA concentrations after i.p. injection of olive oil. $n = 8$. Data represent 2 independent experiments. (**b**) Serum FFA and TG concentrations in fed mice and mice fasted for 24 h. $n = 8$. Data represent 3 independent experiments. (**c**,**d**) Quantification of serum, eWAT (**c**), liver and cardiac (**d**) BODIPY concentrations 3 h after i.p. injection. $n = 8$. Data represent 3 independent experiments. (**e**,**f**) Quantification of serum and eWAT (**e**) and liver and cardiac (**f**) ^{14}C radioactivity after i.p. injection of [^{14}C]oleic acid. Tissue concentrations were measured 2 h after injection. $n = 8$. Data represent 2 independent experiments. (**g**,**h**) Quantification of serum, eWAT (**g**), liver and cardiac (**h**) ^{14}C radioactivity after i.p. injection of [^{14}C]oleic acid and i.p. rMfge8. $n = 5$. Data represent 1 experiment. (**i**) Serum Mfge8 after i.p. rMfge8 in *Mfge8*$^{-/-}$ mice. $n = 5$. Data represent 1 experiment. Female mice were used for all experiments except for those in **i**. $^{\#}P < 0.05$, $^{*}P < 0.01$, $^{**}P < 0.001$, $^{***}P < 0.0001$. Data are expressed as mean ± s.e.m. A Student's *t*-test was used for all statistical analyses except for that in **g** and **h**, where an one-way ANOVA with *post hoc* Bonferroni *t*-test was used.

^{14}C concentrations 2 h after injection as compared with WT controls (**Fig. 3e**,**f**). Injection of rMfge8 i.p. rescued the differences in serum, eWAT, liver and cardiac tissue ^{14}C concentrations in *Mfge8*$^{-/-}$ mice (**Fig. 3g**,**h**). Serum Mfge8 concentrations after i.p. injection peaked at approximately 1.5 µg ml^{-1} 30 min after administration and dropped to baseline concentrations found in WT mice (approximately 2 ng ml^{-1}) 120 min after injection (**Fig. 3i**).

Mfge8 stimulates fatty acid uptake through PI3K

Treatment with rMfge8 induced phosphorylation of Akt at S473 in 3T3-L1 cells, and this effect was blocked by the PI3K (encoded by *Pik3r1*) inhibitor wortmannin (**Fig. 4a**). Wortmannin also inhibited the ability of rMfge8 to increase fatty acid uptake in adipocytes from *Mfge8*$^{-/-}$ mice (**Fig. 4b**). Mfge8-induced phosphorylation of Akt required the discoidin and integrin binding domain of Mfge8 (**Fig. 4c**) and was inhibited by antibodies blocking the α_v, β_3 or β_5 integrin subunits (**Fig. 4d**). Treatment with rMfge8 also induced phosphorylation of As160, an Akt substrate important for fatty acid uptake, in an integrin-dependent manner in 3T3-L1 adipocytes and HepG2 cells (**Fig. 4c**,**e**,**f**).

Next, we found that siRNA-mediated knockdown of the rapamycin-insensitive companion of mTOR (RICTOR) prevented rMfge8 from increasing fatty acid uptake in HepG2 cells (**Fig. 4g**,**h**). Treatment with rMfge8 induced phosphorylation of RICTOR (in both human and mouse cells), and this effect required an intact integrin-binding motif and at least one discoidin domain (**Fig. 4c**,**e**). We also found that siRNA knockdown of RICTOR prevented Mfge8 from inducing phosphorylation of Akt and As160 (**Fig. 4i**). A Pkc-ζ (encoded by *Prkcz*) inhibitor, but not a control inhibitor, prevented the increase in fatty acid uptake induced by Mfge8 in primary adipocytes and HepG2 cells (**Fig. 4j**), as well as in 3T3-L1 adipocytes (**Supplementary Fig. 4e**).

Mfge8 induces cell surface translocation of Cd36 and Fatp1

We next separated cell membrane fractions by ultracentrifugation using a discontinous iodixanol OptiPrep step gradient[25] and identified the fractions most highly enriched for markers of the cell membrane (Atp1a1), Golgi network (Stx6) and endoplasmic reticulum (Calr) by western blot analysis (**Fig. 5a**). We then evaluated selected fractions and found a marked reduction in Cd36 and Fatp1 expression in the Atp1a1 fraction in primary adipocytes from *Mfge8*$^{-/-}$ mice, with a complementary increase in expression of Cd36 in the Stx6-rich membrane fraction and Fatp1 in the Calr-rich fraction as compared with WT controls (**Fig. 5b**). The addition of rMfge8 resulted in similar membrane expression of Cd36 and Fatp1 in adipocytes from *Mfge8*$^{-/-}$ mice to those observed in WT cells (**Fig. 5b**). In 3T3-L1 adipocytes, rMfge8 increased cell surface expression of Cd36 and Fatp1, and this effect was inhibited by wortmannin (**Fig. 5b**). In HepG2 cells, silencing of RICTOR inhibited translocation of CD36 to the cell membrane after rMfge8 treatment (**Fig. 5c**).

We also evaluated Cd36/CD36 translocation in 3T3-L1 adipocytes and HepG2 cells, respectively, by cell surface antibody staining[26]. In 3T3-L1 cells, rMfge8 increased translocation of Cd36 to the cell surface, and translocation was inhibited by both wortmannin and Pkc-ζ inhibitor (**Fig. 5d**). Of note, rMfge8 did not induce Glut4

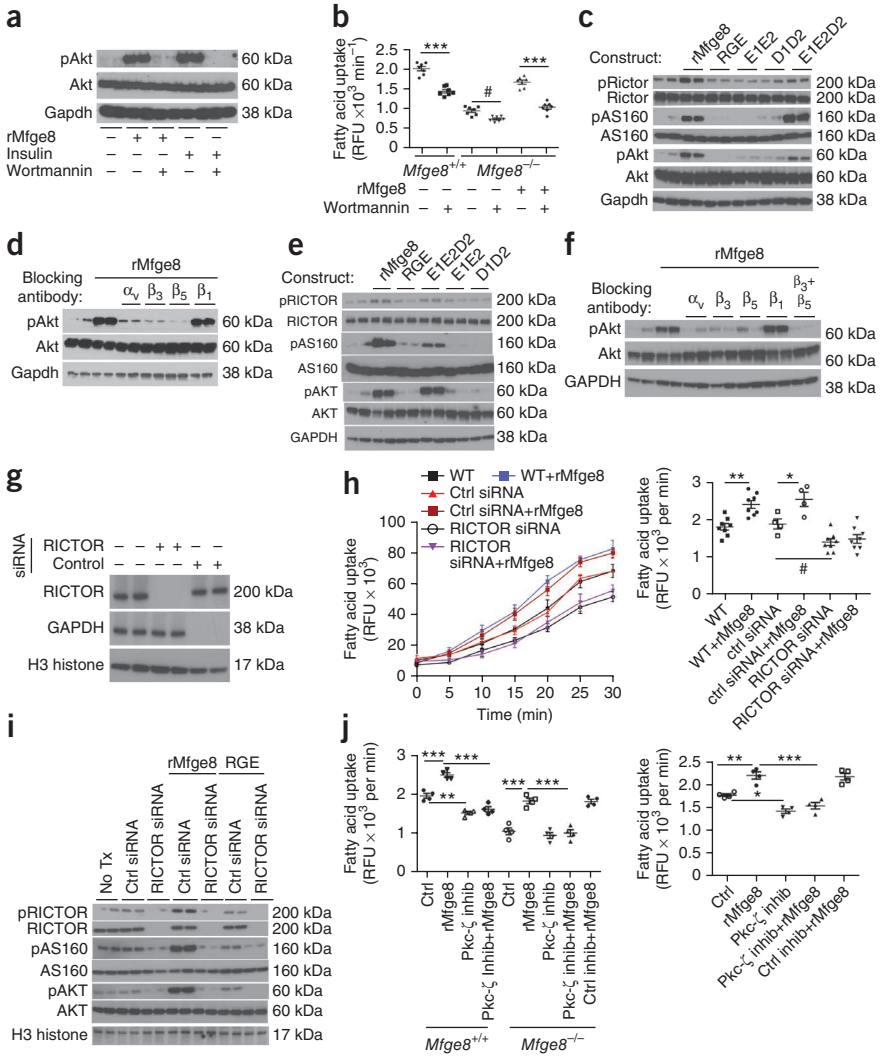

Figure 4 Mfge8 increases fatty acid uptake through PI3K. (**a**) Effect of rMfge8 (10 μg ml^{-1}) or insulin (1 μM) with and without wortmannin (100 nM) on phosphorylation of Akt (pAkt). Gapdh, glyceraldehyde 3-phosphate dehydrogenase (loading control). (**b**) Effect of wortmannin on fatty acid uptake in primary *Mfge8*$^{+/+}$ and *Mfge8*$^{-/-}$ adipocytes and on *Mfge8*$^{-/-}$ adipocytes treated with rMfge8. $n = 7$. (**c**) Effect of mutated Mfge8 constructs on Akt, Rictor and As160 phosphorylation in 3T3-L1 adipocytes. (**d**) Effect of integrin-blocking antibodies on Akt phosphorylation in 3T3-L1 adipocytes treated with rMfge8. (**e**) The effect of mutated Mfge8 constructs on phosphorylation of AKT, RICTOR and AS160 in HepG2 cells. (**f**) The effect of rMfge8 on AKT phosphorylation in the presence of integrin-blocking antibodies in HepG2 cells. α_v, β_3, β_5, β_1, and $\beta_3 + \beta_5$ blocking antibodies. (**g**) Western blot showing efficiency of RICTOR-targeting siRNA and control siRNA (GAPDH) in HepG2 cells. (**h**) Time course (left) and rate (right) of fatty acid uptake in HepG2 cells treated with siRNA targeting RICTOR with or without rMfge8. $n = 8$ for WT and RICTOR siRNA–treated cells and $n = 4$ for control siRNA–treated HepG2 cells. Ctrl, control. (**i**) Western blot for pAKT and pAS160 in HepG2 cells treated with RICTOR siRNA and rMfge8. Tx, treatment. (**j**) Effect of Pkc-ζ or control inhibitor (inhib) on fatty acid uptake in primary *Mfge8*$^{+/+}$ and *Mfge8*$^{-/-}$ adipocytes from female mice (left) and HepG2 cells (right). $n = 4$. $^{\#}P < 0.05$, $^{*}P < 0.01$, $^{**}P < 0.001$, $^{***}P < 0.0001$. Data are expressed as mean ± s.e.m. Each replicate represents an independent experiment. One-way ANOVA with *post hoc* Bonferroni *t*-test was used for all statistical analyses. For western blots, $n = 2$ for each condition, and each blot is representative of 3 independent experiments.

(encoded by *Slc2a4*) translocation to the cell surface in 3T3-L1 adipocytes (**Fig. 5e**). Silencing of RICTOR in HepG2 cells inhibited translocation of CD36 to the cell membrane after rMfge8 treatment (**Fig. 5f**). We confirmed the effect of rMfge8 on Cd36 and Fatp1 translocation in 3T3-L1 adipocytes by confocal microscopy (**Fig. 5g**,**h**).

However, we found that rMfge8 did not increase fatty acid uptake in adipocytes from *Cd36*$^{-/-}$ or *Fatp1*$^{-/-}$ mice (**Fig. 5i**). Further, incubation with a Cd36-blocking antibody prevented rMfge8 from increasing fatty acid uptake in cells from *Mfge8*$^{-/-}$ mice (**Fig. 5j** and **Supplementary Fig. 5a**,**b**). To determine whether Mfge8 induced an increase in total cellular expression of Cd36 and Fatp1, we evaluated the eWAT of *Mfge8*$^{-/-}$ mice on a HFD by western blot analysis. Cd36 and Fatp1 expression was similar in eWAT of from *Mfge8*$^{-/-}$ mice on a HFD as compared with eWAT from WT mice on HFD (**Supplementary Fig. 5c**,**d**). Likewise, rMfge8 did not induce increased expression of either transporter in primary adipocytes or 3T3-L1 cells *in vitro* (**Supplementary Fig. 5e**,**f**).

Mfge8$^{-/-}$ mice are protected from diet-induced obesity

Mfge8$^{-/-}$ mice gained less weight as compared with WT control mice over a 12-week period on a HFD, whereas there was no difference in weight gain between mutant and WT mice on a normal chow diet (**Fig. 6a** and **Supplementary Fig. 6a**,**b**). The eWAT of 20-week-old *Mfge8*$^{-/-}$ mice on a HFD weighed less than control eWAT (**Fig. 6b**). There was a marked induction of Mfge8 protein in eWAT of WT mice on HFD (**Fig. 6c** and **Supplementary Fig. 6c**). 20-week-old *Mfge8*$^{-/-}$ mice on a HFD or normal chow diet had smaller adipocytes and reduced hepatic TG content as compared with WT controls (**Fig. 6d**–**g**). The hearts of *Mfge8*$^{-/-}$ mice also had reduced TG content as compared with WT controls (**Supplementary Fig. 6d**). We also found that 20-week-old *Mfge8*$^{-/-}$ mice on a HFD and 10- and 20-week-old, but not 5-week-old, *Mfge8*$^{-/-}$ mice on a normal chow diet had less total body fat and percentage body fat as compared with WT controls (**Fig. 6h** and **Supplementary Fig. 6e**). Further, 20-week-old *Mfge8*$^{-/-}$ mice on a HFD had increased insulin sensitivity compared with WT controls (**Fig. 6i** and **Supplementary Fig. 6a**,**b**), while 10-week-old, but not 5-week-old, *Mfge8*$^{-/-}$ mice on a normal chow diet had enhanced insulin sensitivity as compared with WT controls (**Supplementary Fig. 6h**,**i**). *Mfge8*$^{-/-}$ mice on HFD had higher stool TG concentrations and caloric content, as measured by bomb calorimetry, as compared with WT controls (**Fig. 6j**).

There was also a marked reduction in eWAT-infiltrating macrophages, as shown by immunohistochemistry (**Supplementary Fig. 7a**,**b**), and a reduction in multiple immune populations, as evaluated by flow cytometry (**Supplementary Fig. 7c**–**i**), in eWAT from *Mfge8*$^{-/-}$ mice as compared with WT controls. There was also no difference in the number or percentage of activated splenic lymphocytes

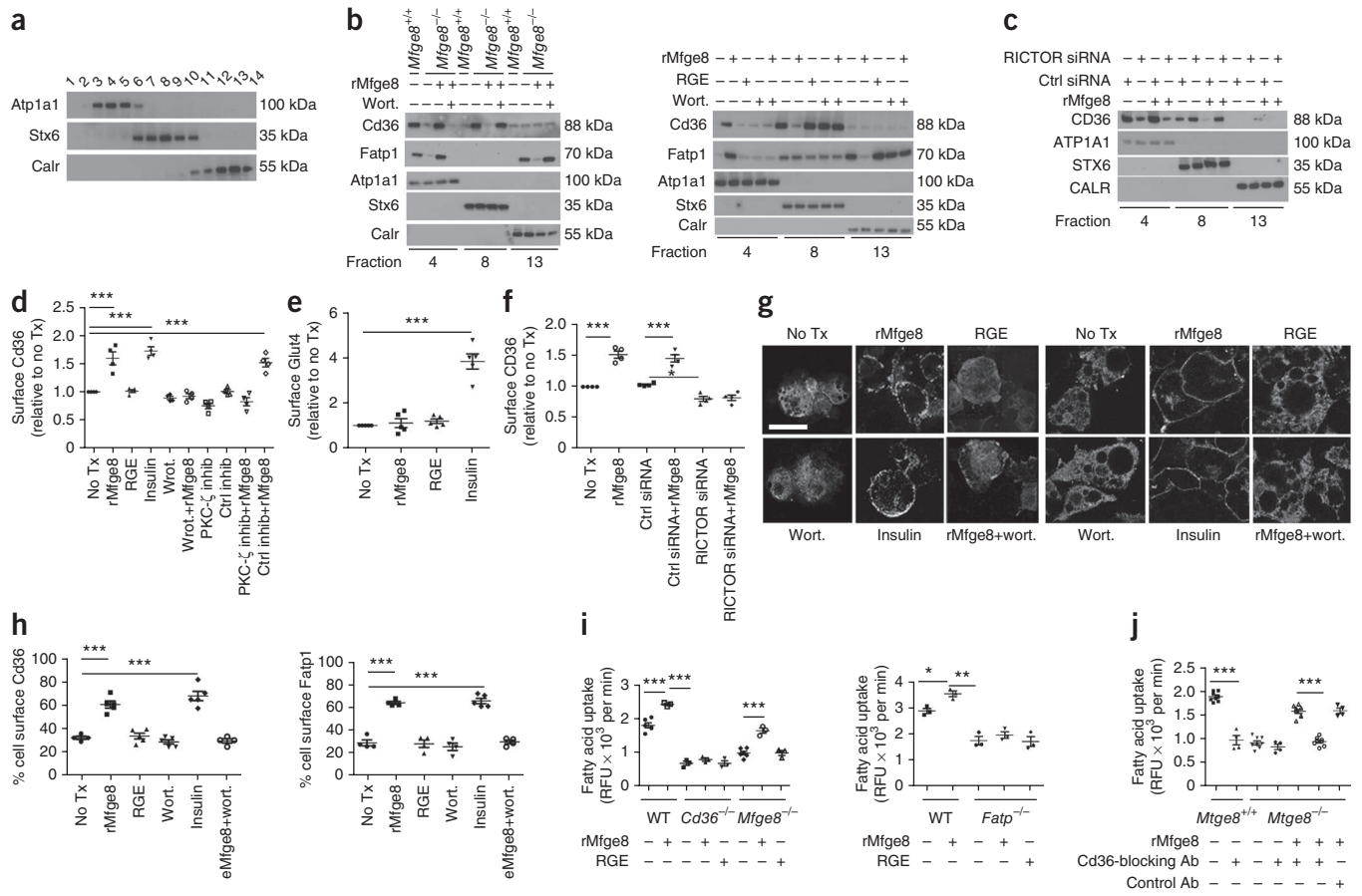

Figure 5 Mfge8 induces cell surface translocation of Cd36 and Fatp1. (**a**) Western blot of membrane fractions probed for expression of Atp1a1, Stx6 and Calr after cell fractionation. (**b**,**c**) Membrane fractions probed for Cd36 and Fatp1 in primary *Mfge8*$^{-/-}$ and *Mfge8*$^{+/+}$ adipocytes and *Mfge8*$^{-/-}$ adipocytes (left) and 3T3-L1 adipocytes (right) treated with rMfge8 with or without wortmannin (Wort.) (**b**) and in HepG2 cells treated with siRNA targeting RICTOR or control siRNA and rMfge8 (**c**). Each western blot represents 3 independent experiments. (**d**) Cell surface Cd36 expression in 3T3-L1 adipocytes in response to rMfge8. $n = 4$. (**e**) Glut4 translocation in 3T3-L1 adipocytes in response to rMfge8. $n = 5$. (**f**) CD36 translocation assay in HepG2 cells treated with siRNA targeting RICTOR or control siRNA and rMfge8. $n = 4$. (**g**,**h**) Confocal images showing cell surface expression (**g**) of Cd36 (left) and Fatp1 (right) and quantification (**h**) of Cd36 and Fatp1 expression after treatment with rMfge8 with or without wortmannin. Scale bar, 50 µm. (Left, no treatment and wortmannin $n = 4$, and rMfge8, RGE, and insulin $n = 5$. Right, $n = 4$ except insulin $n = 5$). (**i**) Effect of rMfge8 on fatty acid uptake in WT and *Cd36*$^{-/-}$ adipocytes (left, $n = 3$ except *Mfge8*$^{-/-}$ and WT, where $n = 5$) and *Fatp1*$^{-/-}$ primary adipocytes (right, $n = 3$). (**j**) Effect of Cd36-blocking or control antibody on fatty acid uptake in primary *Mfge8*$^{-/-}$ and *Mfge8*$^{+/+}$ adipocytes treated with rMfge8. $n = 4$ for experiments with antibodies and 8 for experiments with and without rMfge8. $^{*}P < 0.05$, $^{**}P < 0.001$, $^{***}P < 0.0001$. Data are expressed as mean ± s.e.m. For functional assays, each replicate represents an independent experiment. One-way ANOVA with *post hoc* Bonferroni *t*-test was used for all statistical analyses except for that in **e**, where a Student's *t*-test was used. For western blots, $n = 1$ for each condition and each blot is representative of 3 independent experiments. Male mice were used for these experiments.

or total number of cells in the spleens of 20-week-old *Mfge8*$^{-/-}$ mice on a HFD as compared with WT controls (**Supplementary Fig. 7j**). *Mfge8*$^{-/-}$ mice had fewer TUNEL-positive cells in the eWAT as compared with WT controls (**Supplementary Fig. 8a**).

We next examined energy expenditure in *Mfge8*$^{-/-}$ mice. 12-week-old *Mfge8*$^{-/-}$ and WT mice on HFD for 10 d had no differences in total oxygen consumption, oxygen consumption corrected for lean body mass, food intake or ambulation (**Supplementary Fig. 8b**,**c**). We did find a modestly higher respiratory exchange ratio in *Mfge8*$^{-/-}$ mice without changes in eWAT Ppargc1a expression compared to WT mice (**Supplementary Fig. 8d**,**e**). We also found a modestly higher degree of liver and eWAT 2-deoxy-D-glucose uptake after i.p. injection in *Mfge8*$^{-/-}$ mice as compared with WT controls (**Supplementary Fig. 8f**,**g**). In addition, we evaluated induction of Pdk4 expression in skeletal muscle of mice after a 16-h fast. As expected, Pdk4 expression was induced in fasted WT mice (**Supplementary Fig. 8h**). Pdk4 expression was higher in fed *Mfge8*$^{-/-}$ mice as compared with WT mice, without any further increase in the fasting state.

DISCUSSION

The work presented here identifies a major role for Mfge8 in regulating obesity through modulation of cellular uptake and storage of fatty acids. Mfge8 deficiency leads to fat malabsorption, a reduction in total body fat and protection from diet-induced obesity (DIO). Mfge8 also regulates fatty acid uptake and deposition in the heart, liver and white adipose tissue. Although the *in vivo* sequelae of impaired fatty acid uptake in these organs in *Mfge8*$^{-/-}$ mice is obscured by dietary fat malabsorption, the data suggest that under normal conditions (WT mice and humans), Mfge8 promotes fat uptake in these tissues. This conclusion is supported by the persistent increase in serum TG and FFA concentrations in *Mfge8*$^{-/-}$ mice after i.p. olive oil administration despite an initial reduction in TG and FFA concentrations due

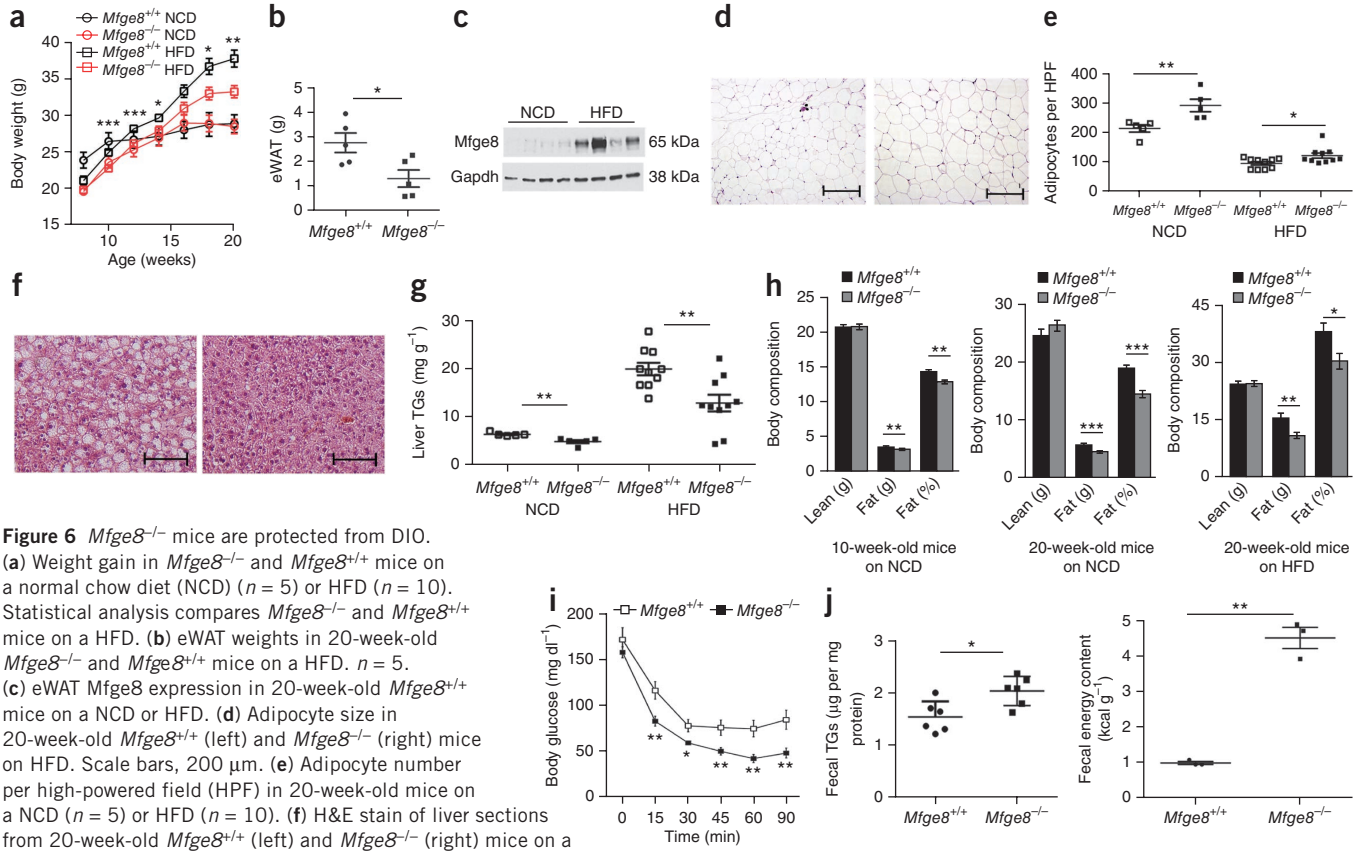

Figure 6 *Mfge8*$^{-/-}$ mice are protected from DIO. (**a**) Weight gain in *Mfge8*$^{-/-}$ and *Mfge8*$^{+/+}$ mice on a normal chow diet (NCD) ($n = 5$) or HFD ($n = 10$). Statistical analysis compares *Mfge8*$^{-/-}$ and *Mfge8*$^{+/+}$ mice on a HFD. (**b**) eWAT weights in 20-week-old *Mfge8*$^{-/-}$ and *Mfge8*$^{+/+}$ mice on a HFD. $n = 5$. (**c**) eWAT Mfge8 expression in 20-week-old *Mfge8*$^{+/+}$ mice on a NCD or HFD. (**d**) Adipocyte size in 20-week-old *Mfge8*$^{+/+}$ (left) and *Mfge8*$^{-/-}$ (right) mice on HFD. Scale bars, 200 μm. (**e**) Adipocyte number per high-powered field (HPF) in 20-week-old mice on a NCD ($n = 5$) or HFD ($n = 10$). (**f**) H&E stain of liver sections from 20-week-old *Mfge8*$^{+/+}$ (left) and *Mfge8*$^{-/-}$ (right) mice on a HFD. Scale bars, 100 μm. (**g**) Liver TG concentrations in 20-week-old mice on a NCD ($n = 5$) or HFD ($n = 10$). (**h**) Body composition of *Mfge8*$^{+/+}$ and *Mfge8*$^{-/-}$ mice aged 10 weeks on a NCD (left, $n = 23$ and $n = 24$, respectively), aged 20 weeks on a NCD (middle, $n = 5$) or aged 20 weeks on a HFD (right, $n = 10$) for 12 weeks. (**i**) Insulin tolerance tests in 20-week-old *Mfge8*$^{+/+}$ and *Mfge8*$^{-/-}$ mice on a HFD. $n = 10$. (**j**) Fecal TG (left, $n = 6$) and energy content (right, $n = 3$) in *Mfge8*$^{+/+}$ and *Mfge8*$^{-/-}$ mice on a HFD. Each sample represents stool combined from 2 mice. Male mice were used for all experiments. For all *in vivo* experiments, each group of 5 mice represents 1 independent experiment. $^{*}P < 0.05$, $^{**}P < 0.01$, $^{***}P < 0.001$. Data are expressed as mean ± s.e.m. A Student's *t*-test was used for statistical analyses.

to impaired dietary absorption, the reduced deposition of BODIPY and [^{14}C]oleic acid in the eWAT, liver and heart of *Mfge8*$^{-/-}$ mice after i.p. injection and the increase in serum TG and FFA concentrations in *Mfge8*$^{-/-}$ mice after starvation-induced lipolysis.

The rate at which fatty acids are taken up can be modified by increases in fatty acid transporter expression, translocation of transporters to the cell membrane and increases in the concentration gradients of fatty acids across cell membranes. Fatty acid transporter translocation is a key regulatory step by which cellular uptake of fatty acids can be acutely modified in response to hormonal and metabolic cues[27]. Insulin and muscle contraction increase fatty acid uptake in skeletal and cardiac muscle through this mechanism[28,29]. The Mfge8-dependent pathway adds an additional layer of regulation of fatty acid uptake through transporter translocation.

Insulin and Mfge8 induce translocation of fatty acid transporters via PI3K[5,30] (**Supplementary Fig. 8i**). To increase glucose uptake, insulin activates the same PI3K-Akt-As160 pathway to translocate Glut4 to the cell surface as for translocation of fatty acid transporters to the cell surface. Notably, Mfge8 activation of this pathway does not increase glucose uptake or Glut4 translocation to the cell surface, suggesting a divergence of the signaling pathways triggered by Mfge8 and insulin downstream of As160 phosphorylation. These data suggest that by increasing fatty acid uptake without directly affecting glucose uptake, the Mfge8 pathway provides a mechanism to dissociate regulation of these two major components of nutrient metabolism. The relative contribution of locally expressed Mfge8 as compared with serum Mfge8 to fatty acid uptake is unclear. Of note, serum concentrations of Mfge8 are markedly lower than the amount expressed in the white adipose tissue of mice on a HFD or concentrations that have been reported in human breast milk (approximately 30–50 μg ml^{-1})[31], suggesting that local expression is likely to have a substantial role in Mfge8 function. However, it is impossible to know for certain from our data whether Mfge8 promotes fatty acid uptake through an autocrine or paracrine mechanism and whether different mechanisms are active in specific tissues.

The relative contribution of Mfge8-mediated Cd36 translocation to increased fatty acid uptake induced by Mfge8 in different organ systems is an area of active investigation. Our data indicate that Mfge8 regulates both Fatp1 and Cd36 translocation in mouse adipocytes. The roles of Cd36 and Fatp1 in promoting fatty acid uptake are well established in adipocytes[32,33] and cardiac myocytes[32,34] and are consistent with a model whereby the effect of Mfge8 on fatty acid uptake in these tissues is mediated through translocation of Fatp1 and Cd36 to the cell surface. Whether the effect of Mfge8 on fatty acid uptake in the intestinal tract is primarily mediated through Cd36 is less clear. Absorption of dietary fats is a multistep process that begins with luminal breakdown of ingested TGs into FFAs that are subsequently taken up by enterocytes, where they are reesterified and secreted as chylomicrons[35]. Cd36 modulates both absorption of dietary fats and secretion of TGs by intestinal epithelial cells[36–38]. The impairment

in *Mfge8*$^{-/-}$ enterocyte fatty acid uptake *in vitro* and the increase in fecal energy content in *Mfge8*$^{-/-}$ mice suggest that the main effect of Mfge8 is to stimulate uptake of fatty acids. As we found in adipocytes, Mfge8 may interact with additional fatty acid transporters in the gastrointestinal tract, leading to overlapping but not identical phenotypes in enteral fat absorption in *Mfge8*$^{-/-}$ and *Cd36*$^{-/-}$ mice. Of note, both Mfge8 and Cd36 mediate apoptotic cell clearance in concert with the $\alpha_v\beta_3$ integrin[9,39]. Whether these processes are linked or involve translocation of Cd36 to the cell surface is unclear.

Our work also identifies a key role for α_v integrins in regulating lipid homeostasis. Previous work has identified a role for the $\alpha_5\beta_1$ and $\alpha_6\beta_1$ integrins in adipocyte differentiation[40]. We show that both the $\alpha_v\beta_3$ and $\alpha_v\beta_5$ integrins regulate fatty acid uptake by inducing Akt phosphorylation via PI3K and mTOR complex 2. Of note, integrins are overexpressed in many malignancies[41], and overexpression is important in the interaction of malignant cells with the extracellular matrix relative to both cancer growth and metastasis[42]. Our data raise the possibility that integrin overexpression in malignancies may increase tumor cell fatty acid uptake. This may be of particular importance in malignancies such as prostate cancer, where cells preferentially metabolize fatty acids[43] and overexpress the $\alpha_v\beta_3$ integrin[44].

Notably, Mfge8 has a number of functions that could potentially contribute to differences in body fat, including regulation of apoptotic cell clearance, inflammation and autoimmunity. *Mfge8*$^{-/-}$ mice develop an age-dependent lupus-like syndrome as a result of chronic immune activation[45]. Chronic disease can lead to a wasting syndrome characterized by cachexia and weight loss and associated with an increased metabolic rate[46]. However, weight loss induced by chronic illness is characterized by loss of both muscle and fat mass[47,48], whereas *Mfge8*$^{-/-}$ mice have an isolated decrease in fat mass without differences in energy expenditure. In addition, *Mfge8*$^{-/-}$ mice do not have evidence for autoimmune disease at 10 weeks of age[45], a time at which they already have less body fat than their WT counterparts.

Obesity is characterized by chronic inflammation with accumulation of apoptotic and necrotic adipocytes[49]. Although one might have expected *Mfge8*$^{-/-}$ mice to have impaired apoptotic adipocyte clearance coupled with increased susceptibility to DIO, we found the opposite phenotype. In fact, these are the first studies, to our knowledge, to demonstrate protection from inflammation in any organ system with Mfge8 deficiency. In addition to the near absence of crown-like structures and reduced numbers of apoptotic cells, adipocyte tissue from *Mfge8*$^{-/-}$ mice on a HFD had fewer activated lymphocytes, regulatory T cells, M1 and M2 macrophages and eosinophils. Although we cannot completely exclude a contribution from some other function of Mfge8 to lipid metabolism, we believe that the combination of impaired *in vitro* fatty acid uptake, impaired *in vivo* TG absorption, partial protection from DIO, normal energy expenditure and protection from adipose tissue inflammation provides evidence to support a major role for Mfge8 in regulation of fat absorption and storage.

Our results also provide a mechanism to explain the recent observations that *MFGE8* is located in a region linked with susceptibility to obesity in humans[19] and that adipose expression of MFGE8 and the α_v and β_5 integrin subunits is increased in human obesity[20]. Collectively, our data indicate that Mfge8 ligation of integrin receptors increases body fat content by regulating the uptake of fatty acids in the alimentary tract and in peripheral tissues.

From the therapeutic viewpoint, delivery of Mfge8 to the small intestine may aid in the treatment of malabsorption syndromes. Alternatively, inhibition of the Mfge8-dependent pathway provides a new therapeutic target for the treatment of obesity that directly inhibits the molecular pathways of fat absorption in the gastrointestinal tract. Whether inhibition of intestinal fatty acid uptake resulting in an increase in stool fatty acids would provide a more tolerable side effect profile for patients as compared with increased stool triglycerides after inhibition of lipoprotein lipase by Orlistat is unclear. Even so, a better understanding of the mechanisms that regulate fat uptake and storage is of considerable interest in the light of the high morbidity, mortality and economic burden associated with obesity and obesity-related disease.

METHODS

Methods and any associated references are available in the online version of the paper.

Note: Any Supplementary Information and Source Data files are available in the online version of the paper.

ACKNOWLEDGMENTS

This research was supported by US National Institutes of Health grant P30 DK 063-7202 and the University of California, San Francisco (UCSF) Diabetes and Endocrinology Research Center and UCSF Cardiovascular Research Institute startup funds (K.A.). We would like to thank K. Nguyen for help with flow cytometry studies, A. Atakilit and D. Sheppard (UCSF Lung Biology Center) for providing integrin-blocking antibodies, R. Silverstein for providing *Cd36*$^{-/-}$ mice (Cleveland Clinic Research Institute) and K. Ashrafi for thoughtful review of the manuscript.

AUTHOR CONTRIBUTIONS

A.K.-S. and W.M. designed and performed *in vivo* and *in vitro* experiments and aided in writing the manuscript. S.S. carried out *in vivo* experiments with obese mice, isolated recombinant protein constructs and performed flow cytometry. Y.Y.C. carried out *in vivo* insulin sensitivity studies. K.T. aided with isolation of primary and pre-adipocytes and measured fecal energy content. Y.Q. aided with metabolic cage studies. S.M.T., A.S. and A.C. aided in the design of experiments and interpretation of results. K.A. designed the study, analyzed the data and wrote the manuscript.

COMPETING FINANCIAL INTERESTS

The authors declare no competing financial interests.

1. Berk, P.D. *et al.* Selective up-regulation of fatty acid uptake by adipocytes characterizes both genetic and diet-induced obesity in rodents. *J. Biol. Chem.* **274**, 28626–28631 (1999).
2. Berk, P.D. *et al.* Uptake of long chain free fatty acids is selectively up-regulated in adipocytes of Zucker rats with genetic obesity and non-insulin-dependent diabetes mellitus. *J. Biol. Chem.* **272**, 8830–8835 (1997).
3. Stump, D.D., Fan, X. & Berk, P.D. Oleic acid uptake and binding by rat adipocytes define dual pathways for cellular fatty acid uptake. *J. Lipid Res.* **42**, 509–520 (2001).
4. Anderson, C.M. & Stahl, A. SLC27 fatty acid transport proteins. *Mol. Aspects Med.* **34**, 516–528 (2013).
5. Stahl, A., Evans, J.G., Pattel, S., Hirsch, D. & Lodish, H.F. Insulin causes fatty acid transport protein translocation and enhanced fatty acid uptake in adipocytes. *Dev. Cell* **2**, 477–488 (2002).
6. Luiken, J.J. *et al.* Insulin induces the translocation of the fatty acid transporter FAT/CD36 to the plasma membrane. *Am. J. Physiol. Endocrinol. Metab.* **282**, E491–E495 (2002).
7. Luiken, J.J. *et al.* Contraction-induced fatty acid translocase/CD36 translocation in rat cardiac myocytes is mediated through AMP-activated protein kinase signaling. *Diabetes* **52**, 1627–1634 (2003).
8. Atabai, K. *et al.* Mfge8 is critical for mammary gland remodeling during involution. *Mol. Biol. Cell* **16**, 5528–5537 (2005).
9. Hanayama, R. *et al.* Identification of a factor that links apoptotic cells to phagocytes. *Nature* **417**, 182–187 (2002).
10. Greenberg, M.E. *et al.* Oxidized phosphatidylserine-CD36 interactions play an essential role in macrophage-dependent phagocytosis of apoptotic cells. *J. Exp. Med.* **203**, 2613–2625 (2006).
11. Nandrot, E.F. *et al.* Essential role for MFG-E8 as ligand for $\alpha_v\beta_5$ integrin in diurnal retinal phagocytosis. *Proc. Natl. Acad. Sci. USA* **104**, 12005–12010 (2007).
12. Ryeom, S.W., Sparrow, J.R. & Silverstein, R.L. CD36 participates in the phagocytosis of rod outer segments by retinal pigment epithelium. *J. Cell Sci.* **109**, 387–395 (1996).

13. Tandon, N.N., Kralisz, U. & Jamieson, G.A. Identification of glycoprotein IV (CD36) as a primary receptor for platelet-collagen adhesion. *J. Biol. Chem.* **264**, 7576–7583 (1989).
14. Atabai, K. *et al.* Mfge8 diminishes the severity of tissue fibrosis in mice by binding and targeting collagen for uptake by macrophages. *J. Clin. Invest.* **119**, 3713–3722 (2009).
15. Kudo, M. *et al.* Mfge8 suppresses airway hyperresponsiveness in asthma by regulating smooth muscle contraction. *Proc. Natl. Acad. Sci. USA* **110**, 660–665 (2013).
16. Silvestre, J.S. *et al.* Lactadherin promotes VEGF-dependent neovascularization. *Nat. Med.* **11**, 499–506 (2005).
17. Aziz, M.M. *et al.* MFG-E8 attenuates intestinal inflammation in murine experimental colitis by modulating osteopontin-dependent $\alpha_v\beta_3$ integrin signaling. *J. Immunol.* **182**, 7222–7232 (2009).
18. Twito, T., Madeleine, D., Perl-Treves, R., Hillel, J. & Lavi, U. Comparative genome analysis with the human genome reveals chicken genes associated with fatness and body weight. *Anim. Genet.* **42**, 642–649 (2011).
19. Rankinen, T. *et al.* The human obesity gene map: the 2005 update. *Obesity (Silver Spring)* **14**, 529–644 (2006).
20. Henegar, C. *et al.* Adipose tissue transcriptomic signature highlights the pathological relevance of extracellular matrix in human obesity. *Genome Biol.* **9**, R14 (2008).
21. Aoki, N. *et al.* Identification and characterization of microvesicles secreted by 3T3–L1 adipocytes: redox- and hormone-dependent induction of milk fat globule-epidermal growth factor 8-associated microvesicles. *Endocrinology* **148**, 3850–3862 (2007).
22. Yu, F. *et al.* Proteomic analysis of aorta and protective effects of grape seed procyanidin b2 in *db/db* mice reveal a critical role of milk fat globule epidermal growth factor-8 in diabetic arterial damage. *PLoS ONE* **7**, e52541 (2012).
23. Cheng, M. *et al.* Correlation between serum lactadherin and pulse wave velocity and cardiovascular risk factors in elderly patients with type 2 diabetes mellitus. *Diabetes Res. Clin. Pract.* **95**, 125–131 (2012).
24. Liao, J., Sportsman, R., Harris, J. & Stahl, A. Real-time quantification of fatty acid uptake using a novel fluorescence assay. *J. Lipid Res.* **46**, 597–602 (2005).
25. Pohl, J., Ring, A., Korkmaz, U., Ehehalt, R. & Stremmel, W. FAT/CD36-mediated long-chain fatty acid uptake in adipocytes requires plasma membrane rafts. *Mol. Biol. Cell* **16**, 24–31 (2005).
26. Samovski, D., Su, X., Xu, Y., Abumrad, N.A. & Stahl, P.D. Insulin and AMPK regulate FA translocase/CD36 plasma membrane recruitment in cardiomyocytes via Rab GAP AS160 and Rab8a Rab GTPase. *J. Lipid Res.* **53**, 709–717 (2012).
27. Bonen, A., Luiken, J.J., Arumugam, Y., Glatz, J.F. & Tandon, N.N. Acute regulation of fatty acid uptake involves the cellular redistribution of fatty acid translocase. *J. Biol. Chem.* **275**, 14501–14508 (2000).
28. Jain, S.S. *et al.* Additive effects of insulin and muscle contraction on fatty acid transport and fatty acid transporters, FAT/CD36, FABPpm, FATP1, 4 and 6. *FEBS Lett.* **583**, 2294–2300 (2009).
29. Glatz, J.F., Luiken, J.J. & Bonen, A. Membrane fatty acid transporters as regulators of lipid metabolism: implications for metabolic disease. *Physiol. Rev.* **90**, 367–417 (2010).
30. Chabowski, A. *et al.* Insulin stimulates fatty acid transport by regulating expression of FAT/CD36 but not FABPpm. *Am. J. Physiol. Endocrinol. Metab.* **287**, E781–E789 (2004).
31. Newburg, D.S. *et al.* Role of human-milk lactadherin in protection against symptomatic rotavirus infection. *Lancet* **351**, 1160–1164 (1998).
32. Coburn, C.T. *et al.* Defective uptake and utilization of long chain fatty acids in muscle and adipose tissues of CD36 knockout mice. *J. Biol. Chem.* **275**, 32523–32529 (2000).
33. Wu, Q. *et al.* FATP1 is an insulin-sensitive fatty acid transporter involved in diet-induced obesity. *Mol. Cell. Biol.* **26**, 3455–3467 (2006).
34. Tanaka, T. *et al.* Defect in human myocardial long-chain fatty acid uptake is caused by FAT/CD36 mutations. *J. Lipid Res.* **42**, 751–759 (2001).
35. Bamba, V. & Rader, D.J. Obesity and atherogenic dyslipidemia. *Gastroenterology* **132**, 2181–2190 (2007).
36. Drover, V.A. *et al.* CD36 mediates both cellular uptake of very long chain fatty acids and their intestinal absorption in mice. *J. Biol. Chem.* **283**, 13108–13115 (2008).
37. Drover, V.A. *et al.* CD36 deficiency impairs intestinal lipid secretion and clearance of chylomicrons from the blood. *J. Clin. Invest.* **115**, 1290–1297 (2005).
38. Nassir, F., Wilson, B., Han, X., Gross, R.W. & Abumrad, N.A. CD36 is important for fatty acid and cholesterol uptake by the proximal but not distal intestine. *J. Biol. Chem.* **282**, 19493–19501 (2007).
39. Moodley, Y. *et al.* Macrophage recognition and phagocytosis of apoptotic fibroblasts is critically dependent on fibroblast-derived thrombospondin 1 and CD36. *Am. J. Pathol.* **162**, 771–779 (2003).
40. Liu, J., DeYoung, S.M., Zhang, M., Cheng, A. & Saltiel, A.R. Changes in integrin expression during adipocyte differentiation. *Cell Metab.* **2**, 165–177 (2005).
41. Mizejewski, G.J. Role of integrins in cancer: survey of expression patterns. *Proc. Soc. Exp. Biol. Med.* **222**, 124–138 (1999).
42. Zhao, Y. *et al.* Tumor $\alpha_v\beta_3$ integrin is a therapeutic target for breast cancer bone metastases. *Cancer Res.* **67**, 5821–5830 (2007).
43. Liu, Y., Zuckier, L.S. & Ghesani, N.V. Dominant uptake of fatty acid over glucose by prostate cells: a potential new diagnostic and therapeutic approach. *Anticancer Res.* **30**, 369–374 (2010).
44. Zheng, D.Q., Woodard, A.S., Fornaro, M., Tallini, G. & Languino, L.R. Prostatic carcinoma cell migration via $\alpha_v\beta_3$ integrin is modulated by a focal adhesion kinase pathway. *Cancer Res.* **59**, 1655–1664 (1999).
45. Asano, K. *et al.* Masking of phosphatidylserine inhibits apoptotic cell engulfment and induces autoantibody production in mice. *J. Exp. Med.* **200**, 459–467 (2004).
46. Poehlman, E.T., Scheffers, J., Gottlieb, S.S., Fisher, M.L. & Vaitekevicius, P. Increased resting metabolic rate in patients with congestive heart failure. *Ann. Intern. Med.* **121**, 860–862 (1994).
47. Bonetto, A. *et al.* STAT3 activation in skeletal muscle links muscle wasting and the acute phase response in cancer cachexia. *PLoS ONE* **6**, e22538 (2011).
48. Rolland, Y., Abellan van Kan, G., Gillette-Guyonnet, S. & Vellas, B. Cachexia versus sarcopenia. *Curr. Opin. Clin. Nutr. Metab. Care* **14**, 15–21 (2011).
49. Strissel, K.J. *et al.* Adipocyte death, adipose tissue remodeling, and obesity complications. *Diabetes* **56**, 2910–2918 (2007).

ONLINE METHODS

Mice. All animal experiments were approved by the UCSF Institutional Animal Care and Use Committee in adherence to US National Institutes of Health guidelines and policies. *In vivo* studies were conducted with two different lines of mice deficient in Mfge8. Studies in **Figures 3g–i** and **6a–i** and **Supplementary Figures 5c**,**d**, **6c–e**,**h**,**i**, **7**, **8a** and **12** were carried out on *Mfge8*$^{-/-}$ mice created by a gene disruption vector[8,16]. Mice were backcrossed ten generations into the C57BL/6 background and bred as *Mfge8*$^{-/-}$ breeding pairs and *Mfge8*$^{+/+}$ breeding pairs. In a subset of studies (**Supplementary Fig. 6a**,**g**), *Mfge8*$^{-/-}$ and *Mfge8*$^{+/-}$ breeding pairs were used to generate sibling littermates from the same cage. A second line of Mfge8-lacking mice created by homologous recombination was obtained from RIKEN[9]. These mice were bred as *Mfge8*$^{-/-}$ and *Mfge8*$^{+/-}$ breeding pairs and used in studies in **Supplementary Figure 6b**,**h** and as *Mfge8*$^{-/-}$ and *Mfge8*$^{+/+}$ breeding pairs for studies used in **Figures 2**, **3**, and **6j** and **Supplementary Figures 1**, **3**, **4** and **8b–h** and for harvesting of all primary cells used in *in vitro* studies. All mice were age- (6–10 weeks of age unless otherwise noted) and sex-matched. β_3- and β_5-deficient mice in the 129 SVEV strain have been previously described[50,51]. *Cd36*$^{-/-}$ mice were provided by R. Silverstein and were in the C57BL/6 background. *Fatp1*$^{-/-}$ mice were also in the C57BL/6 background[33]. For **Figure 2c–f**, investigators were blinded to genotypes until statistical analysis of the data. Investigators were not blinded as to genotype in animal studies that involved weighing mice on a high-fat diet, obtaining insulin tolerance tests and determining body composition by dual-energy X-ray absorptiometry (DEXA) scan. Investigators were blinded to the mouse genotypes for the energy expenditure experiments, which were performed by the UCSF Diabetes and Endocrinology Research Center Metabolic Research Unit.

Fatty acid uptake assay. We assessed uptake of fatty acids by primary cells and cell lines using a QBT Fatty Acid Uptake Kit (Molecular Devices). We plated cells in triplicate in 96-well plates at a concentration of 25,000 cells per well in 100 µl of DMEM with 10% FCS. We centrifuged plates at 1,000 r.p.m. for 4 min and incubated at 37 °C for 4–5 h. We then serum-deprived cells for 1 h before treatment with recombinant proteins for 30 min followed by the addition of QBT Fatty Acid Uptake solution. In experiments using function-blocking antibodies or cyclic RGD and RAD, we added 20 µg ml^{-1} antibodies against mouse integrins α_v (clone RMV-7, Abcam)[52], β_3 (clone 2C9.G2; BD Biosciences)[53], β_5 (clone ALULA, provided by A. Atakilit)[54], β1 (clone HA2/5; BD Biosciences, raised against rat with crossreactivity with mouse)[55] and Cd36 (clone MF3; Abcam)[56] and human integrins α_v (clone L230, provided by A. Atakilit)[57], β_3 (clone Axum-2)[51], β_5 (clone ALULA), β1 (clone P5D2), cyclo-RGD (10 µg ml^{-1}) and cyclo-RAD (10 µg ml^{-1}) (Bachem) to cells after serum deprivation, and we incubated cells for 20 min at 4 °C before addition of recombinant proteins. In experiments using pharmacological inhibitors, we incubated cells with wortmannin (100 ng ml^{-1}, Abcam), Pkc-ζ inhibitor (a pseudosubstrate, 5 µM concentration, BML-P219-500, Enzo Life Sciences) or Pkc-ζ control inhibitor (a scrambled pseudosubstrate, 5 µM concentration, 63695, ANASPEC) for 20 min. We incubated plates in a fluorescent plate reader at 37 °C and acquired kinetic readings every 20 s for 30 min. We plotted fluorescence values against time and expressed data as relative fluorescent units (RFU) per min × 10^3 measured 30 min after the assay was begun.

Cell culture. We differentiated 3T3-L1 (Zen-Bio) fibroblasts into adipocytes as described previously[24]. Briefly, we cultured 3T3-L1 fibroblasts on 10-cm tissue culture plates or in six-well tissue culture dishes in DMEM supplemented with 10% FBS and 25 mM HEPES (normal medium). 2 d after the cells reached confluence, we changed the medium to differentiation medium (DMEM with 10% FBS with the addition of 3-isobutyl-1-methylxanthine (Calbiochem), dexamethasone (Sigma) and insulin (Sigma) at concentrations of 0.5 mM, 1 µM and 1 µM, respectively) to induce adipocyte differentiation. After differentiation, we maintained cells for 2 d in culture medium supplemented with 1 µM insulin and subsequently in DMEM supplemented with 10% FCS. We confirmed differentiation by observing lipid droplets in >75% of cells and harvested cells for use 6–10 d after differentiation. We propagated the human hepatocellular carcinoma cell line HepG2 in Eagle's MEM supplemented with 10% FBS .

3T3-L1 cell triglyceride content assay. We plated 3T3-L1 fibroblasts in equal densities in 10-cm tissue culture plates in DMEM supplemented with 10% FBS and allowed them to grow to confluence. 48 h after reaching confluence differentiation, we added medium with or without rMfge8 or RGE construct (10 µg ml^{-1}). After 48 h, we replaced the differentiation medium with culture medium supplemented with 1 µM insulin with and without recombinant protein constructs. Subsequently, we maintained cells in DMEM supplemented with 10% FCS (DMEM with 10% FBS) and recombinant protein constructs and replaced medium every 48 h. On days 2, 4, 6 and 8 after differentiation, we trypsinized cells and placed them into a 1.5-ml tube, adding a 2.5-fold volume of 2:1 chloroform/methanol. We homogenized samples by running them through a 25-gauge syringe and sonicating for 5 s, after which we added 0.2 volume of methanol. We vortexed samples for 30 s, followed by centrifugation at 1,000*g* for 15 min. We collected the supernatant in a new tube and added 0.2 volumes of 0.04% $CaCl_2$ and centrifuged at 500*g* for 15 min. We discarded the upper phase and washed the interphase three times with wash buffer (3% chloroform, 48% methanol) followed by centrifugation each time for 15 min at 500*g*. We added 50 µl of methanol after the final wash. We dried and dissolved samples in 50 µl 3:2 *t*-butanol/Triton X-100 and quantified using a TG determination kit (Sigma-Aldrich TR100).

Primary cell culture. We obtained primary mouse adipocytes from epididymal fat pads by collagenase digestion in Krebs-HEPES (KRBH) buffer followed by filtering through a 100-µm strainer, which we subsequently washed with an additional 7.5 ml KRBH buffer. We allowed adipocytes to float to the top of the mixture for 5 min and removed the solution under the adipocyte layer with a syringe. We washed the adipocytes with 10 ml KRBH and again allowed them to float to the surface; we then removed the solution again. We repeated this process 3 times and resuspended and counted cells from 0.5–1.0 ml.

We isolated and cultured mouse adipocyte progenitors from the vascular stromal fraction as reported previously[58]. In brief, we removed subcutaneous white adipose tissue, minced and digested tissue with 1 mg ml^{-1} collagenase for 45 min at 37 °C in DMEM/F12 medium containing 1% bovine serum albumin (BSA) and antibiotics. We then filtered digested tissue through a sterile 150-µm nylon mesh and centrifuged at 250*g* for 5 min. We discarded the floating fractions consisting of adipocytes and resuspended the pellet containing the stromal vascular fractions in buffer (154 mM NH_4Cl, 10 mM $KHCO_3$, 0.1 mM EDTA) for 10 min. We further centrifuged cells at 500*g* for 5 min, plated at 8 × 10^5 per well of a 24-well plate and grew them in 37 °C in DMEM/F12 supplemented with 10% FBS at 37 °C. 2 d after cells reached 100% confluence, we treated cells with 1 µM rosiglitazone and 1 µM insulin to induce terminal differentiation.

We obtained primary hepatocytes by perfusing the liver through the portal vein with calcium-free buffer (0.5 mM EDTA, HBSS without Ca^{2+} and Mg^{2+}) and next perfused with collagenase (3.5 U ml^{-1} Collegenase II from Worthington, 25 mM HEPES, HBSS with Ca^{2+} and Mg^{2+}). We purified parenchymal cells with Percoll buffer (90% Percoll (Sigma), 1 × PBS) at low-speed centrifugation (1,500 r.p.m. for 10 min). We plated cells in collagen-I–coated dishes and cultured at 37 °C in a humidified atmosphere of 95% O_2 and 5% CO_2 in growth medium[59].

We collected primary enterocytes by harvesting the proximal small intestine from anesthetized mice, emptied the luminal contents, washed with 115 mM NaCl, 5.4 mM KCl, 0.96 mM NaH_2PO_4, 26.19 mM $NaHCO_3$ and 5.5 mM glucose buffer at pH 7.4 and gassed for 30 min with 95% O_2 and 5% CO_2. We then filled the proximal small intestines with buffer containing 67.5 mM NaCl, 1.5 mM KCl, 0.96 mM NaH_2PO4, 26.19 mM $NaHCO_3$, 27 mM sodium citrate and 5.5 mM glucose at pH 7.4, saturated with 95% O_2 and 5% CO_2, and incubated in a bath containing oxygenated saline at 37 °C with constant shaking. After 15 min, we discarded the luminal solutions and filled the intestines with buffer containing 115 mM NaCl, 5.4 mM KCl, 0.96 mM NaH_2PO_4, 26.19 mM $NaHCO_3$, 1.5 mM EDTA, 0.5 mM dithiothreitol and 5.5 mM glucose at pH 7.4, saturated with 95% O_2 and 5% CO_2, and we placed them in saline as described above. After 15 min, we collected and centrifuged the luminal contents (1,500 r.p.m., 5 min, room temperature) and resuspended the pellets in DMEM saturated with 95% O_2 and 5% CO_2 (ref. 60).

We harvested primary cardiac myocytes by immersing hearts in ice-cold calcium-free perfusion buffer containing (in mM) NaCl 120.4, KCl 14.7, KH_2PO_4 0.6, Na_2HPO_4 0.6, 5 $MgSO_4$-$7H_2O$ 1.2, Na-HEPES 10, $NaHCO_3$ 4.6, taurine 30, butanedione monoxime 10 and glucose 5.5 and then perfused via the aorta with calcium-free perfusion buffer (3 ml min^{-1}) for 4 min; we then

doi:10.1038/nm.3450

switched to calcium-free digestion buffer (perfusion buffer containing 2 mg ml^{-1} collagenase II) for 10 min. We then perfused with digestion buffer containing 100 μM $CaCl_2$ for another 8–10 min. We removed hearts from the perfusion apparatus and placed in a 10-cm Petri dish containing 2 ml digestion buffer and 3 ml stop buffer (perfusion buffer supplemented with 10% FBS). We removed the atria and the ventricles and cut into 10–12 equally sized pieces. We then gently dispersed the tissue into cell suspension using plastic transfer pipettes. We collected the cell suspension in a 15-ml Falcon tube, brought to 10 ml with stop buffer and centrifuged at 40*g* for 3 min. We removed to damaged myocytes and nonmyocytes by a series of washes in 10 ml stop buffer containing, sequentially, 100, 400 or 900 μM $CaCl_2$. We pelleted cardiomyocytes by centrifugation at 40*g* for 3 min after each wash and plated in laminin-coated dishes[61].

Primary cell viability. We stained freshly isolated primary cells with annexin V-FITC (BD Biosciences) and propridium iodide and assessed cell viability by flow cytometry.

Recombinant protein production. We created and expressed recombinant protein constructs in High Five cells as previously described[14]. All constructs were expressed with a human Fc domain for purification across a protein G sepharose column. For studies using different recombinant constructs, we used the molar equivalent of 10 μg ml^{-1} of full-length recombinant Mfge8. We used full-length recombinant protein, or mutated constructs, containing a human Fc domain for all studies except to set up the standard curve in **Supplementary Figure 6c**, where we used commercial recombinant protein (R&D).

Fat absorption assays. We fasted 6- to 8-week-old mice for 4 h and then gavaged with olive oil (15 μl per g body weight). Mice had access to water but not food for the remainder of the experiment. In the experiments in **Figure 2c**,**e**, we mixed 50 μg per kg body weight of recombinant protein into olive oil and administered immediately to mice by gavage. In blocking antibody experiments, we administered antibodies to α_v (clone RMV-7, Abcam) and β_5 (clone ALULA, provided by A. Atakilit) by gavaging mice with 100 μl water containing 0.5 μg per g body weight 30 min before olive oil gavage. We measured serum TG and FFA concentrations using a commercially available kit (Sigma-Aldrich,Wako[62]). We measured serum Mfge8 concentrations with Mfge8 DuoSet ELISA development kit according to the manufacturer's instructions (R&D Systems). In some experiments, we treated mice with an i.p. injection of Triton WR-1339 (200 mg per kg body weight) 30 min before olive oil gavage with subsequent measurement of TG concentrations. In some experiments, we injected mice with i.p. olive oil (200 μl) with subsequent measurement of serum TG and FFA concentrations.

Triglyceride content. 8 h after olive oil gavage, we isolated samples from the left lobe of the liver and the proximal small intestine and rapidly froze them in liquid nitrogen for TG content assays depicted in **Supplementary Figure 3a**,**c**,**d**. We measured TG content of the liver from mice on HFD from livers isolated in fed mice. We quantified TG content of the intestine[63], liver[64] and fecal samples[64] as described previously and standardized to the weight of the tissue.

Glucose gavage. We fasted 6 to 8-week-old mice for 4 or 18 h and then gavaged with glucose (1.5 mg per g body weight). In the experiments in **Figure 2i**, we mixed 50 μg per kg body weight of recombinant protein into glucose solution and administered immediately to mice by gavage. In blocking antibody experiments (**Fig. 2j**), we administered α_v (clone RMV-7, Abcam) and β_5 (clone ALULA, provided by A. Atakilit) antibodies orally with 100 μl water containing 0.5 μg per g body weight 30 min before glucose gavage. We measured blood glucose concentrations by sampling from the tail vein of mice from 0–60 min after glucose was administered.

Boron-dipyrromethene gavage. We fasted 6- to 8-week-old mice for 4 h and then each mouse received 2 μg per g body weight BODIPY and 2 μg per g body weight rhodamine-PEG (Methoxyl PEG Rhodamine B, MW 5,000 g mol^{-1}) with 0.2% fatty acid–free BSA by gavage. We collected feces from 20 min to 4 h after BODIPY was administered. We homogenized 50 mg of feces in PBS containing 30 mM HEPES, 57.51 mM MgCl2 and 0.57 mg ml^{-1} BSA with 0.5% SDS and sonicated for 30 s; we then centrifuged at 1,000*g* for 10 min. We transferred supernatants to 96-well plates and measured fluorescence values immediately using a fluorescence microplate reader for endpoint reading (Molecular Devices). We also measured serum BODIPY and rhodamine concentrations from blood drawn 4 h after gavage. For both measurements, we subtracted baseline fluorescence from untreated mice from measured fluorescence. For BODIPY, the excitation and emission wavelengths were 488 nm and 515 nm, respectively. For rhodamine-PEG, the excitation and emission wavelengths were 575 nm and 595 nm, respectively.

Boron-dipyrromethene. We fasted mice for 4 h and injected them with 15 μl g^{-1} BODIPY solution containing quencher (Molecular Devices) or control solution (HBSS supplemented with 20 mM HEPES and 0.2% FFA free BSA) in a total volume of 200 μl. At indicated time points, we euthanized mice and harvested the liver, eWAT and heart and homogenized in RIPA buffer, centrifuged and read the fluorescence signal in the supernatant using a plate reader with an excitation wavelength of 485 nm and an emission wavelength of 525 nm. We subtracted the fluorescence signal from each tissue and in serum from mice treated with control solution from the appropriate BODIPY-treated samples. For BODIPY measurements in the liver, eWAT and cardiac tissue, we normalized measured concentrations to the weight of the extracted tissue.

[^{14}C]oleic acid. We fasted mice for 4 h and gave a 200-μl i.p. injection of olive oil containing 2 μCi [^{14}C]oleic acid. In some experiments, we injected mice with rMfge8 (100 μg per kg body weight) i.p. 2 min before [^{14}C]oleic acid injection. Prior to and 30, 60, 90 and 120 min after [^{14}C]oleic acid administration, we drew 10 μl blood from the tail vein. We harvested eWAT, heart and liver after the last time point. We minced 200 mg liver, 150 mg eWAT and whole hearts and place them in glass scintillation vials. We dissolved the tissues and serum in tissue solubilizer (Biosol, National Diagnostic) (1 ml for tissues and 10 μl for serum) in 50 °C shaking water bath (3 h for tissues and 1 h for serum). We then decolorized samples by incubation with 0.3 ml 30% hydrogen peroxide for 1 h in room temperature for tissue samples and at 50 °C for blood samples. We added scintillation solution (Bioscint, National Diagnostic) to each vial (10:1 vol/vol). We measured ^{14}C content by liquid scintillation normalized to mg of tissue or μl of serum.

Western blot. For signaling studies, we grew 3T3-L1 adipocytes, and HepG2 cells in DMEM supplemented with 10% FCS, serum starved for 1 h and treated them with and without rMfge8 constructs (10 μg ml^{-1}) for 15 min. In studies using pharmacological inhibitors or blocking antibodies, we incubated cells with the appropriate inhibitor for 20 min before the addition of any recombinant protein constructs. In brief, we lysed all cells and tissues in cold RIPA buffer (50 mM Tris HCl pH 7.5, 150 mM NaCl, 1% NP-40, 1% sodium deoxycholate, 0.1% SDS) supplemented with complete miniprotease and phosphatase inhibitor cocktail (Pierce, Rockford, IL). We incubated cell or tissue lysates at 4 °C with gentle rocking for 15 min or 1 h, respectively, sonicated on ice for 30 s and then centrifuged at 12,800 r.p.m. for 15 min at 4 °C. We determined protein concentration by Bradford assay (Bio-Rad, Hercules, CA). We separated 20 μg of protein by SDS-PAGE on 7.5% resolving gels (Bio-Rad) and transblotted onto polyvinylidene fluoride membranes (Millipore). We incubated the membranes with a 1:1,000 dilution of antibodies against Akt (catalog 9272, Cell Signaling), Rictor (clone 53A2, Cell Signaling), As160 (catalog 2447, Cell Signaling), α_v integrin (clone RMV-7, Abcam), β_3 integrin (clone 2C9.G2, BD Biosciences), β_5 integrin (clone ALULA, provided by A. Atakilit), Cd36 (clone FA6-152, Novus Biologicals), Fatp1 (clone I-20, Santa Cruz), Ppargc1a (clone 81B8, Cell Signaling), phospho-Akt Ser473 (clone 193H12, Cell Signaling), Phospho-Rictor Thr1135 (clone D30A3, Cell Signaling), phospho-As160 (catalog 4288, Cell Signaling), Gapdh (clone 14C10, Cell Signaling) or Mfge8 (catalog AF2805, R&D Systems). For evaluation of total Akt, Rictor and As160, we stripped and reprobed membranes that been blotted for phospho-Akt, phospho-Rictor and phospho-As160.

Cell fractionation. We performed cell fractionation as previously described[25] by discontinuous OptiPrep step gradient with modification. We placed primary adipocytes and 3T3-L1 cells in serum-free conditions for 40 min, after which they were treated with recombinant protein constructs and/or inhibitors for 20 min

under serum-free conditions. We washed cells in PBS and then homogenized (Tissue Tearor Model 985370) in buffer containing 25 mM sucrose, 0.5 mM EDTA in 10 mM Tris and then centrifuged at 1,000*g* for 5 min to remove cell debris. We resuspended the supernatant with homogenization buffer and then passed it ten times through a 25-gauge syringe needle and homogenized again. We then centrifuged the homogenate at 2,000*g* for 10 min to obtain a postnuclear supernatant, which we then centrifuged at 100,000 *g* for 1 h in homogenization buffer containing 25% (wt/vol) iodixanol. We put the resulting suspension in a 9-step OptiPrep gradient (AXIS-Shield, Oslo, Norway) consisting of 1%, 4%, 7%, 10%, 13%, 16%, 19%, 22% and 25% iodixanol and centrifuged in Beckman L8-55 ultracentrifuge using a SW41Ti rotor at 200,000*g* for 3 h at 4 °C. We collected 14 fractions from the bottom of each tube by aspiration using a syringe with a metal filling cannula (1.2 mm, Becton Dickinson). We analyzed one-quarter of each fraction by western blotting with 1:1,000 dilution of antibodies directed against Atp1a1 (catalog 3010, Cell Signaling), Stx6 (clone C34B2, Cell Signaling) and Calr (clone EPR3924, Millipore) (**Fig. 5a**). We used the fractions that had the highest expression of Atp1a1 (4), Stx6 (8) and Calr (13) for subsequent studies examining translocation of Cd36 and Fatp1.

Cd36 and Glut4 translocation. We evaluated translocation of Cd36 and Glut4 to the cell surface as previously described[26]. We serum-starved 3T3-L1 adipocytes for 12 h and treated with rMfge8 or RGE construct (10 μg ml^{-1}), insulin (1 μM), wortmannin (100 nM) or Pkc-ζ or control inhibitor (5 μM) for 20 min. We then fixed cells with 3% paraformaldehyde and blocked for 1 h with blocking buffer (PBS, 0.05% Tween 20, 1% BSA, 5% goat serum). We then incubated cells with rat antibody against mouse Cd36 (Abd Serotec, MCA2748) or Glut4 (N-20, Santa Cruz, D2613) at a concentration of 1:500, followed by a secondary horseradish peroxidase–conjugated antibody (Santa Cruz) at a concentration of 1:1,000, followed with 3,3′,5,5′-Tetramethylbenzidine Liquid Substrate System (TMB, Sigma) at room temperature, after which we terminated the reaction with 1 N NaOH and read with a plate reader (Molecular Devices, SpectraMax M2) at 450 nm. We subsequently rinsed cells with PBS and incubated with wheat germ agglutinin Alexa Fluor 680 conjugate (WGA Alexa-680, Invitrogen) for 30 min, washed again with PBS and used Odyssey infrared imager (Licor) to read the signal at 700 nm. We subtracted background signals from the infrared signal as well as from controls read by TMB immunostaining with primary antibodies omitted from the raw data.

siRNA. We maintained the HepG2 cells in minimum essential medium supplemented with 10% FBS at 37 °C under 5% CO_2. We plated HepG2 cells in six-well plates 1 d before infection. We transfected cells with 100 nM RICTOR siRNA (ON-TARGETplus Human RICTOR, 253260, Thermo Fisher Scientific) or controls (ON-TARGETplus GAPDH Control siRNA, Human, Thermo Fisher Scientific) in antibiotic- and norepinephrine-free culture medium using Lipofectamine-2,000 (Invitrogen). 6 h later, we change the medium to fully supplemented medium and conducted assays 48 h after transfection.

RNA extraction and quantitative RT-PCR. We purified total RNA from mouse quadriceps muscles by guanidinium thiocyanate-phenol-chloroform extraction. Briefly, we homogenized tissues in TRIsure (Bioline BIO-38033) and mixed with 1-bromo-3-chloropropane. After centrifugation, we mixed aqueous phase with 2-propanol to precipitate RNA. The precipitate was pelleted by centrifugation and washed with ethanol. We analyzed RNA with NanoDrop 2000 (Thermo) to determine purity and quantity and used 1 μg of RNA for first-strand cDNA synthesis (Quanta 95048). We performed quantitative RT-PCR using SensiFast SYBR green (Bioline) on the CFX384 Real Time PCR system (BioRAD). We expressed data as relative expression of Pdk4 mRNA by comparative threshold method using 36B4 as the internal control. We used the following primers: Pdk4 forward 5′-CCGCTGTCCATGAAGCA-3′, reverse 5′-GCAGAAAAGCAAAGGACG TT-3′ and 36B4 forward 5′-GCAGACAACGTGGGCTCCAAGCAGAT-3′, reverse 5′-GGTCCTCCTTGGTGAACACGAAGCCC-3′.

High-fat diet. We placed 8- to 10-week-old mice on a high-fat formula containing 60% fat calories (Research Diets) for 12 weeks. The control diet contained 9% fat calories (PMI). We housed mice in groups of 5 mice per cage for diet experiments including body weight measurements, insulin tolerance tests, DEXA scanning for body composition, adipocyte size quantification and hepatic TG content, with each cage of 5 mice representing an independent experiment.

Immunohistochemistry and TUNEL assay. We cleared 5-μm paraffin-embedded sections with xylene, rehydrated and boiled them for 20 min and passively cooled them for 20 min in 10 mM sodium citrate (pH 6) for antigen retrieval. For immunoperoxidase staining, we blocked sections with H_2O_2 in methanol and subsequently 2% BSA. For fluorescent staining, we blocked sections in TBS with 0.5% Tween 20, 10% goat serum and 5% BSA. We used rabbit antibody against Lgals3 (clone M3/38, Cedarlane) at 1:3,800 dilution in TBS with 0.5% Tween 20, followed by a 1:200 biotinylated antibody against rabbit IgG (catalog BA-1000, Vector), ABC reagent (Vector) and liquid diaminobenzidine substrate (Sigma). We used rabbit antibody against Tjp1 (catalog mab1520, Chemicon) at 1:200, followed by Alexa Fluor 568–conjugated goat antibody against rabbit IgG (catalog A-21069, Molecular Probes) at 1:500 in Immunostain Enhancer (Pierce). We quantified TUNEL-positive cells in eWAT of mice on a HFD from tissue sections stained with Apoptag Fluorescein kit (Millipore, S7160) following manufacturer's instructions.

Immunocytochemistry and confocal microscopy. We cultured 3T3-L1 cells on glass coverslips, fixed cells for 20 min in Z-fix (Anatech) and blocked in TBS with 0.5% Tween 20, 10% goat serum and 5% BSA. We permeabilized cells with 0.5% Triton X-100 in TBS and added rat antibody against Cd36 (clone MF3, Abcam) and goat antibody against Fatp1 (clone I-20, Santa Cruz) at 1:200 in Immunostain Enhancer (Pierce), followed by secondary antibodies Alexa Fluor 488– conjugated goat antibody against rat IgG (catalog A-11006, Molecular probes) and Alexa Fluor 488–conjugated donkey antibody against goat IgG (catalog A-11055, Molecular probes) at 1:500 in TBS with 0.5% Tween 20, 10% goat serum and 5% BSA. We mounted coverslips with fluorescent mounting medium (DakoCytomation; Carpinteria, CA). We performed confocal microscopy using a 40× oil objective lens on a Zeiss LSM 510 laser-scanning confocal microscope and processed images using ImageJ software.

Morphometric analysis. To quantify adipocyte size, we stained paraffin-embedded eWAT sections from 5 chow-diet–fed and 10 HFD-fed mice with H&E. We took 5 high-power field (HPF) pictures for each section at 100× magnification. We counted the average number of adipocytes per HPF for each section and measured the diameter of each adipocyte using Image-Pro Plus MDA. We blinded investigators to the genotype during quantification. For quantification of apoptosis, we quantified TUNEL-positive cells per total nuclei from 5 randomly selected 20× fields. For quantification of Cd36 and Fatp1 staining, we used the Raw Integrated Density (RawIntDen) obtained in ImageJ 1.48f to determine the intensity of total staining of a cell and the intensity of staining inside the plasma membrane. Subtracting the two values gave the intensity of staining at the plasma membrane, which we expressed as a percentage of the total staining for the cell. For each experiment, we analyzed 2 or 3 cells using this method.

Flow cytometry. We dissected, weighed and placed epididymal fat pads in a buffered collagenase solution for homogenization using a GentleMACS tissue dissociator. We incubated homogenized tissue at 37 °C on a rotating shaker at 250 r.p.m. for 30 min then passed it through a 40-μm strainer and rinsed with 10 ml ice-cold PBS. After a red blood cell lysis step, we stained cells for viability using a LIVE/DEAD aqua fixable stain kit (Invitrogen, Carlsbad, CA) and then used 1:200 dilutions of primary conjugated antibodies to the following proteins to identify macrophage subtype and eosinophil populations: Cd45 (clone 30-F11, BioLegend, San Diego, CA), Cd11b (clone M1/70, BioLegend), F4/80 (clone BM8, BioLegend), Cd11c (clone N418, BioLegend), Mgl2 (clone ER-MP23, AbdSerotec, Oxford, United Kingdom) and Siglec5 (clone E50-2440, BD Pharmingen, San Diego, CA). We stained a second set of cells from the fat pads for viability and then used 1:200 dilutions of primary conjugated antibodies to the following proteins to identify lymphocyte populations: Cd45, Cd4 (clone RM4-4, BioLegend), Cd44 (clone IM7, Ebioscience), Cd62L (clone MEL-14, BD Pharmingen), and Foxp3 (clone FJK-16s, Ebioscience, San Diego, CA). After euthanizing mice, we dissected spleens and pushed them through a 40-μm strainer and treated to lyse red blood cells. We subsequently stained splenocytes for viability and the lymphocyte markers detailed above. We performed

doi:10.1038/nm.3450

flow cytometry on a BD FACSVerse flow cytometer and analyzed using FlowJo Software (Tree Star, Ashland, Oregon).

Body composition analysis. We performed bone, lean and fat mass analysis with a GE Lunar PIXImus II Dual Energy X-ray Absorptiometer.

Comprehensive lab animal monitoring system metabolic cage analysis. We placed mice in single housing cages for 5 d before initiating comprehensive lab animal monitoring system (CLAMS) experimental analysis for a period of 96 h. We placed mice on a HFD for 10 d before initiating the analysis. We measured the following variables: food and water intake, oxygen consumption (VO_2) and carbon dioxide production (VCO_2) at 13-min intervals and locomotor activity. Infrared beams monitored movement in the *x*, *y* and *z* directions. The data presented was from the last 48 h of the analysis[65].

Measurements of fecal energy content. We freeze-dried feces from mice on a HFD (samples from 2 mice were combined for each sample) and pulverized them with a ceramic mortar and pestle. We measured caloric content of feces with an 1108 Oxygen Combustion Bomb calorimeter.

Insulin tolerance tests. For insulin tolerance tests, we fasted mice for 5 h, after which we injected them with 1.5 U kg^{-1} of insulin i.p. and collected blood from the tail vein immediately before injection and then again after 15, 30, 60 and 90 min for evaluation of blood glucose.

***In vivo* glucose uptake assay.** We measured glucose uptake *in vivo* using a previously described method[66] with modifications and with the Abcam Glucose Uptake Assay Kit. Briefly, we injected 10-week-old mice i.p. with 2-deoxy-D-glucose (2-DG, 5 mmol per kg body weight in saline) or saline. 45 min after i.p. injection, we euthanized mice and isolated adipocytes, cardiomyocytes and hepatocytes as described for primary cells. We transferred equal numbers of isolated cells into new tubes, washed cells three times with PBS and incubated with KRBH buffer (20 mM HEPES, 5 mM KH_2PO_4, 1mM $CaCl_2$, 136 mM NaCl, 4.7 mM KCl, pH 7.4) with 2% BSA for 20 min. We then lysed cells with cold RIPA buffer, snap-froze them in liquid nitrogen and then heated samples to 90 °C for 15 min. We centrifuged cell lysates at 500 r.p.m. for 2 min and cooled on ice for 5 min. We neutralized samples by adding Neutralization Buffer solution (from Abcam Glucose Uptake Assay Kit), centrifuged lysates again at 1,000 r.p.m. for 3 min., measured the protein concentration by Bradford assay and added 50 µl of each supernatant to 96-well plates. We added 50 µl of Reaction Mix (from Abcam Glucose Uptake Assay Kit) to each well and mixed by pipetting. After incubating at 37 °C for 30 min, we measured 2-DG content of samples using a fluorescence plate reader (Molecular Device).

Statistical analyses. We assessed data for normal distribution and similar variance between groups using GraphPad Prism 6.0. We used a one-way ANOVA to make comparisons between multiple groups. When the ANOVA comparison was statistically significant ($P < 0.05$), we performed further pairwise analysis using a Bonferroni *t*-test. We used a two-sided Student's *t*-test for comparisons between 2 groups. We used GraphPad Prism 6.0 for all statistical analyses. We presented all data as mean ± s.e.m. We selected sample size for animal experiments based on numbers typically used in the literature. We did not perform randomization of animals. We performed all *in vitro* measurements (TG, FFA and glucose concentrations and Mfge8 ELISA) with 3 technical replicates. No statistical method was used to predetermine sample size.

50. Huang, X., Griffiths, M., Wu, J., Farese, R.V. Jr. & Sheppard, D. Normal development, wound healing, and adenovirus susceptibility in β_5-deficient mice. *Mol. Cell. Biol.* **20**, 755–759 (2000).
51. Su, G. *et al.* Absence of integrin $\alpha_v\beta_3$ enhances vascular leak in mice by inhibiting endothelial cortical actin formation. *Am. J. Respir. Crit. Care Med.* **185**, 58–66 (2012).
52. Takahashi, K. *et al.* A murine very late activation antigen-like extracellular matrix receptor involved in CD2- and lymphocyte function-associated antigen-1–independent killer-target cell interaction. *J. Immunol.* **145**, 4371–4379 (1990).
53. Ashkar, S. *et al.* Eta-1 (osteopontin): an early component of type-1 (cell-mediated) immunity. *Science* **287**, 860–864 (2000).
54. Su, G. *et al.* Integrin $\alpha_v\beta_5$ regulates lung vascular permeability and pulmonary endothelial barrier function. *Am. J. Respir. Cell Mol. Biol.* **36**, 377–386 (2007).
55. Zovein, A.C. *et al.* β_1 integrin establishes endothelial cell polarity and arteriolar lumen formation via a Par3-dependent mechanism. *Dev. Cell* **18**, 39–51 (2010).
56. Helming, L., Winter, J. & Gordon, S. The scavenger receptor CD36 plays a role in cytokine-induced macrophage fusion. *J. Cell Sci.* **122**, 453–459 (2009).
57. Thomas, G.J., Hart, I.R., Speight, P.M. & Marshall, J.F. Binding of TGF-β1 latency-associated peptide (LAP) to $\alpha_v\beta_6$ integrin modulates behaviour of squamous carcinoma cells. *Br. J. Cancer* **87**, 859–867 (2002).
58. Tseng, Y.H. *et al.* New role of bone morphogenetic protein 7 in brown adipogenesis and energy expenditure. *Nature* **454**, 1000–1004 (2008).
59. Huang, P. *et al.* Induction of functional hepatocyte-like cells from mouse fibroblasts by defined factors. *Nature* **475**, 386–389 (2011).
60. Anwar, K., Iqbal, J. & Hussain, M.M. Mechanisms involved in vitamin E transport by primary enterocytes and *in vivo* absorption. *J. Lipid Res.* **48**, 2028–2038 (2007).
61. Smyth, J.W. *et al.* Actin cytoskeleton rest stops regulate anterograde traffic of connexin 43 vesicles to the plasma membrane. *Circ. Res.* **110**, 978–989 (2012).
62. Rabot, S. *et al.* Germ-free C57BL/6J mice are resistant to high-fat-diet–induced insulin resistance and have altered cholesterol metabolism. *FASEB J.* **24**, 4948–4959 (2010).
63. Uchida, A. *et al.* Reduced triglyceride secretion in response to an acute dietary fat challenge in obese compared to lean mice. *Front. Physiol.* **3**, 26 (2012).
64. Kim, K.Y. *et al.* Parkin is a lipid-responsive regulator of fat uptake in mice and mutant human cells. *J. Clin. Invest.* **121**, 3701–3712 (2011).
65. Sutton, G.M. *et al.* Diet-genotype interactions in the development of the obese, insulin-resistant phenotype of C57BL/6J mice lacking melanocortin-3 or -4 receptors. *Endocrinology* **147**, 2183–2196 (2006).
66. Ueyama, A., Sato, T., Yoshida, H., Magata, K. & Koga, N. Nonradioisotope assay of glucose uptake activity in rat skeletal muscle using enzymatic measurement of 2-deoxyglucose 6-phosphate *in vitro* and *in vivo*. *Biol. Signals Recept.* **9**, 267–274 (2000).